Adsorption of Perfluoroalkyl Substances (PFAS) in Groundwater by Granular Activated Carbons: Roles of Hydrophobicity of PFAS and Carbon Characteristics

Minkyu Park[a,*], Shimin Wu[a,b], Israel J. Lopez[a], Joseph Y. Chang[a], Tanju Karanfil[c], and Shane A. Snyder[a,d,**]

a. Department of Chemical & Environmental Engineering, University of Arizona, 1133 E James E Rogers Way, Harshbarger 108, Tucson, AZ 85721-0011, USA
b. IER Environmental Protection Engineering Technology Co., Ltd., Shenzhen 518071, China
c. Department of Environmental Engineering and Earth Sciences, Clemson University, Anderson, SC 29625, USA
d. Nanyang Technological University, Nanyang Environment & Water Research Institute (NEWRI), Singapore 637141

[*] Corresponding author: minkyupark@email.arizona.edu
[**] Corresponding author: snyders2@email.arizona.edu

Abstract

The adsorption breakthrough behavior of nine perfluoroalkyl substances (PFAS) in groundwaters by four bituminous coal-based granular activated carbons (F400, Carbsorb 40, HPC and CMR400) was studied using rapid small-scale column tests (RSSCTs). The half breakthrough bed volume (BV_{50}), an indicator of apparent adsorption capacity, correlated with the hydrophobicity of PFAS at a given pH (i.e., Log D_{ow}) for F400, indicating that hydrophobic interaction is important for apparent adsorption capacity of PFAS in groundwater with low dissolved organic concentrations (DOC < 1 mg C/L) and low specific UV absorbances at 254 nm ($SUVA_{254}$ < 2 $L \cdot mg^{-1}m^{-1}$). Higher empty bed contact time (EBCT) caused steeper PFAS breakthrough curves with respect to throughput, but did not affect apparent adsorption capacity. Three different sizes of F400 (0.13, 0.17, and 0.20 mm) exhibited similar breakthrough profiles of PFAS, indicating that the intraparticle diffusivity was independent of adsorbent diameter in the given conditions. Among the tested carbons, the positively charged adsorbents (F400, HPC, and CMR400) showed higher apparent adsorption capacities for hydrophilic (Log D_{ow} at pH 7<0) and marginally hydrophobic PFAS (Log D_{ow} at pH 7 between 0 and 1) than the negatively charged adsorbent (Carbsorb 40). In addition, activated carbons with higher micropore surface areas exhibited higher apparent adsorption capacities of hydrophilic and marginally hydrophobic PFAS among the positively-charged activated carbons, whereas the mesoporous carbon (HPC) exhibited an increasingly larger adsorption capacity for more hydrophobic PFAS compared to the microporous carbon (F400) at a later breakthrough possibly due to less pore blockage.

Keywords: PFAS; Granular Activated Carbon; Groundwater; RSSCT; Breakthrough; Hydrophobicity

1. Introduction

Per- and polyfluoroalkyl substances (PFAS) are a class of aliphatic organofluorine compounds in which the hydrogens are either partially or fully substituted by a fluorine. PFAS possess unique properties such as chemical/thermal stability, and a hydrophilic-lipophilic nature, all of which are desirable for specific commercial applications such as stain repellants, fire-fighting foams, non-stick cookware, and food contact papers. While such chemical properties make PFAS useful and attractive as commercial products, their chemical stability is undesirable in the environment because it renders them persistent (Quiñones and Snyder 2009). Ubiquitous occurrence of PFAS in drinking water supplies was found in Hu et al.'s study, which reported that at least one sample over their sampling campaigns of 66 public water supplies that serve six million people had perfluorooctanoic acid (PFOA) or perfluorooctane sulfonate (PFOS) concentrations at or above the U.S. Environmental Protection Agency (USEPA) health advisory level (70 ng/L individually or combined) (Hu et al. 2016). In addition, perfluoro-2-propoxypropanoic acid (PFPrOPrA, also called "GenX"), a PFAS of emerging concern, was detected at concentrations of up to ~4500 ng/L downstream of a PFAS manufacturing site (Sun et al. 2016). Some states in the U.S. have more stringent notification levels than the USEPA health advisory levels. For instance, recently in August 2019, the California State Water Resources Control Board's Division of Drinking Water established new drinking water notification levels of 5.1 ng/L and 6.5 ng/L for PFOA and PFOS, respectively, based upon available analytical techniques and toxicological information regarding the liver and immune system (SWRCB 2019). Recently, the USEPA announced plans for a national drinking water regulatory determination of PFOA and PFOS, including setting their maximum contaminant levels (MCLs) (EPA 2019). While PFOA and PFOS are of the greatest regulatory concerns, another PFAS, perfluorononanoic acid (PFNA) is being regulated

by the New Jersey Department of Environmental Protection (NJDEP), which has recently established an MCL of 13 ng/L (NJDEP 2018).

Adsorption is one of the most practical and efficacious treatment technologies for the removal of PFAS from water, particularly for long-chain ones (Appleman et al. 2014). While adsorption processes for PFAS removal have widely been studied, only PFAS such as PFOA and PFOS have been focused on likely because these were predominantly produced until they were phased out. Regulatory focus on PFOA and PFOS would be another major reason for the plethora of PFOA and PFOS research. Another limitation of the existing studies is that the majority of the studies provides isotherm testing results without accounting for transport phenomena of PFAS in a fixed-bed adsorber (Carter and Farrell 2010, Hansen et al. 2010, Senevirathna et al. 2010, Yu et al. 2012, Yu et al. 2009), the predominant mode of operation in activated carbon adsorption (Chowdhury 2013).

Ideally, pilot-testing should be utilized because it can best represent a full-scale fixed-bed adsorber since it accounts for heterogeneity of adsorbent sizes and pore blocking by dissolved organic matter, which cannot be easily simulated with bench-scale testing or a numerical simulation (Corwin and Summers 2010). Recently, McCleaf et al. conducted a pilot-scale GAC adsorber test with an empty bed contact time (EBCT) of 6.1 min for assessing the breakthrough of 14 PFAS spiked in groundwater (McCleaf et al. 2017). Another recent pilot-scale study employed an EBCT of 10 min for 10 PFAS in groundwater (Liu et al. 2019). While both studies shed light on the understanding of realistic PFAS breakthrough profiles, it is practically challenging to use pilot-testing to design a full-scale fixed-bed adsorber because of the extended timeframe required to generate a full breakthrough profile. This is particularly true for long-chain hydrophobic PFAS. More practical and applicable approaches, yet less precise, are to use 1) a

numerical simulation with isotherm data, or 2) a rapid small-scale column test (RSSCT) based on a similitude approach (Crittenden et al. 1986). Numerical simulations have been used to predict PFAS breakthrough behavior in full-scale treatment scenarios in the past (Patterson et al. 2019, Xiao et al. 2017). This approach is particularly useful when isotherm data are available; however, it is inevitable that kinetic parameters such as the mass transfer coefficient, surface diffusion coefficient, and pore diffusion coefficient should be estimated. Furthermore, the predictive capabilities of these models are greatly dependent on the parameter estimation (Athanasaki et al. 2015, Worch 2008). The RSSCT is a widely adopted experimental approach that simulates the breakthrough of compounds of interest in a full-scale adsorber. Two similitude models can be used for RSSCT design based on intraparticle diffusion dependency on adsorbent size: constant diffusivity (CD) and proportional diffusivity (PD). The primary benefits of the RSSCT include 1) short experimental duration, 2) small volume of water required for experiments, and 3) no need for extensive experiments for isotherm or kinetic data acquisition (Crittenden et al. 1987). These benefits allow convenient testing for various experimental conditions simulating a full-scale adsorber in a reasonable timeframe without complicated mathematical or numerical modeling.

The main objectives of this study were 1) to evaluate if CD approach is suitable for designing RSSCT in a groundwater, 2) to provide breakthrough behaviors of nine PFAS and their comparisons on four different GACs, and 3) to establish correlations between PFAS physicochemical properties, activated carbon characteristics, and breakthrough behavior. To this end, groundwaters spiked with nine PFAS at individual concentrations of ~350 ng/L were tested since groundwater is a major drinking water source and many groundwater PFAS contamination cases have been reported (Cousins et al. 2016).

2. Materials and Methods

2.1. Rapid small-scale column testing (RSSCT)

RSSCTs were designed based on the constant diffusivity (CD) model. The rationale of the CD model selection is explained in Section 3.1. Four bituminous coal-based activated carbons obtained from Calgon Carbon Corporation—Filtrasorb 400 (F400), Carbsorb 40, HPC Super 8x30 (HPC), and CMR400—with different surface characteristics such as pore surface area and surface charge were selected for the RSSCT since such activated carbon characteristics influence adsorption kinetics and capacity of PFAS (Siriwardena et al. 2019); their physical properties are summarized in Table 1. The selected activated carbons were crushed with mortar and pestle and sieved using U.S. standard sieves with the mesh size of #70, 80, 100 and 140 to obtain the desired particle diameters for small columns. Mean particle diameters (MPDs) of pristine carbons were provided by Calgon Carbon Corporation (Table 1) whereas the mean values of two mesh opening values of two corresponding sieves were calculated as MPDs of crushed carbons for small columns. The crushed activated carbons were thoroughly washed with ultrapure water and stored in a sterile environment until use. The slurry of carbon was then placed in a 10 mm inner diameter column with polypropylene caps and fittings (Kimble Chase, New Jersey). The selection of column dimension considered the minimization of channeling effects (i.e., ratio of column diameter to activated carbon particle diameter should be > 50). The same hydraulic loading (i.e., 3.8 m/hr) was applied for all the tested conditions, which resulted in the Reynolds number (Re) ranging from 0.30 to 0.46 depending on the carbon particle diameters (Tables S4 to S6 in the supplementary material). Each subsection of Section 3 shows results from the combination of activated carbon type, adsorbent diameter, and RSSCT design parameters like

EBCT to explain various aspects of PFAS adsorption in a fixed-bed adsorber. Therefore, RSSCT design parameters for each section were separately specified in Tables S4 to S6 in the supplementary material.

Table 1 Mean particle diameter (MPD), Brunauer–Emmett–Teller (BET) surface distribution, pore volume distribution, and pH at point of zero charge (pH_{PZC}) of the tested activated carbons

Adsorbent	Mean particle diameter (mm)[a]	BET surface area (m^2/g)	BET surface area distribution (m^2/g)			Total pore Volume (cm^3/g)	Pore volume distribution (cm^3/g)			pH_{PZC}
			< 2 nm	2 - 50 nm	> 50 nm		< 2 nm	2 - 50 nm	> 50 nm	
F400	1.122	769	617	143	9	0.41	0.33	0.08	0.00	9.95
Carbsorb40	1.413	755	535	219	1	0.40	0.28	0.12	0.00	7.05
HPC 8x30	1.005	788	451	336	1	0.31	0.18	0.13	0.00	9.05
CMR400[b]	1.015	767	530	224	13	0.41	0.29	0.12	0.01	10.00

a. MPD values were provided by Calgon Carbon Corporation
b. custom municipal reactivated carbon that underwent a steam reactivation (McNamara et al. 2018)

RSSCT experiments used groundwater collected from a tap at the Water & Energy Sustainable Technology (WEST) center located in Tucson, AZ, USA. Two sampling campaigns were conducted. The feed waters for the first and second campaigns had dissolved organic carbon (DOC) concentrations of 0.78 mg/L and 0.53 mg/L, respectively, with corresponding specific UV absorbances at 254 nm [$SUVA_{254}$] of 1.34 $L \cdot mg^{-1}m^{-1}$ and 1.45 $L \cdot mg^{-1}m^{-1}$, respectively. pH of both waters was 7.2. The experiments in sections 3.2 and 3.3 used water from the first campaign; those in sections 3.1 and 3.4 used water from the second campaign. The collected groundwaters were stored in 1000L HDPE tank and left until residual chlorine dissipated. Subsequently, ~350±75 ng/L of PFAS was spiked in the collected water. A multi-channel peristaltic pump was then used to supply the PFAS-containing waters to the activated carbon

columns. The RSSCT lasted for about two weeks and no noticeable degradation of PFAS was observed over the course of sampling (Fig. S3).

2.2. Measurements of pH_{PZC}, surface area, and pore volume distribution

pH of point of zero charge (pH_{PZC}), surface area, and pore size distribution were measured as described elsewhere (Dastgheib et al. 2004). In brief, 100 mg of activated carbons were added into 20 mL 0.1 M NaCl solutions with different initial pH values ranging from 2 to 11 adjusted with 0.5 N HCl or NaOH solutions. Before making the solution, distilled and deionized water was boiled to remove dissolved CO_2. Sealed vials were shaken for 48 h at 200 rpm at room temperature. Subsequently, the final pH of the supernatant of the solution was measured when the carbons were completely settled. If the pH of the NaCl solution did not change after contact with a carbon, that pH was selected as pH_{PZC} of the carbon. The averaged values of two measurements with ±0.2 variation were reported.

For surface area and pore size distribution measurements, adsorption isotherms of nitrogen at relative pressure ranging from 10^{-6} to 1 at 77 K were used (Dastgheib et al. 2004). Subsequently, Brunauer–Emmett–Teller (BET) calculation and Micromeritics' Density Functional Theory (DFT) software with the graphite model with slit shape geometry were used to calculate surface area and pore size distribution, respectively. Results with relative standard deviations less than 3% were accepted and reported.

2.3. DOC analysis

DOC was measured using a Shimadzu total organic carbon (TOC) analyzer (Japan). Samples were filtered before analysis using 0.45 μm syringe filters (PVDF Millex-HV, EMD Millipore) and acidified with hydrochloric acid (37%, ACS grade, Sigma-Aldrich) to pH 2-3.

2.4. Measurement of PFAS

Nine PFAS (Table 2) were analyzed using ultra-high performance liquid chromatography-tandem mass spectrometer (LC-MS/MS) with a high-throughput direct aqueous injection method. Isotope dilution was implemented by spiking stable isotopically-labeled PFBA, PFHxA, PFOA, PFDA, and PFOS into samples to achieve 250 ng/L. An Agilent 1260 binary LC pump equipped with an Agilent ZORBAX RRHD Eclipse Plus C-18 column (100 mm × 2.1 mm, 1.8 µm) was used for chromatographic separation. 5 mM ammonium acetate in HPLC water (A) and methanol (B) were used as the mobile phase with a flow rate of 0.4 mL/min. Single fragment per each analyte was measured using an Agilent 6490 MS/MS system with multiple reaction monitoring mode. The detailed information on mobile phase gradient, method optimization parameters, compound transitions, and relevant QA/QC are available in Sections S1 and S2 in the supplementary material).

Table 2 Names, abbreviations, number of carbons, structures, octanol-water partition coefficient (Log K_{ow}), octanol-water partition coefficient at pH 7 (Log D_{ow} at pH 7), bulk diffusivity (D), and minimal/maximal projection diameter values of the tested PFAS

Compound, Number of carbons	Structure	Log K_{ow}[a]	Log D_{ow} at pH7[a]	D[b] (cm^2/sec)	Minimal/ maximal projection diameter (nm)[a]
Perfluorobutanoic acid (PFBA), C4	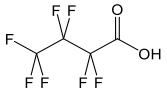	2.31	-1.22	7.89×10^{-6}	0.64 / 0.92
Perfluoropentanoic acid (PFpeA), C5	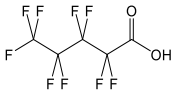	3.01	-0.52	7.19×10^{-6}	0.66 / 1.0
Perfluorohexanoic acid (PFHxA), C6	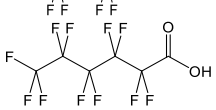	3.71	0.18	6.58×10^{-6}	0.72 / 1.1
Perfluoroheptanoic acid (PFHpA), C7	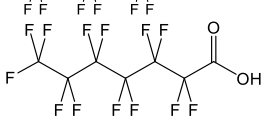	4.41	0.88	6.06×10^{-6}	0.82 / 1.2

Perfluorooctanoic acid (PFOA), C8	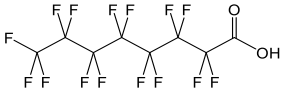	5.11	1.58	5.63×10^{-6}	0.78 / 1.3
Perfluorodecanoic acid (PFDA), C10	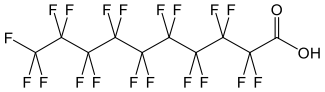	6.51	2.98	4.93×10^{-6}	0.78 / 1.6
Perfluorododecanoic acid (PFDoDA), C12	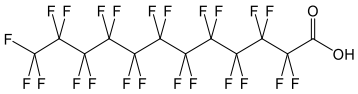	7.92	4.39	4.40×10^{-6}	0.80 / 1.8
Perfluorobutanesulfonic acid (PFBS), C4	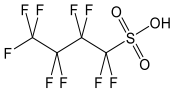	2.63	0.25	7.15×10^{-6}	0.70 / 1.0
Perfluorooctanesulfonic acid (PFOS), C8	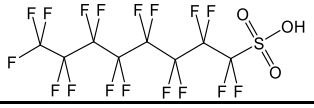	5.43	3.05	5.21×10^{-6}	0.80 / 1.3

a. Estimated data obtained using MarvinSketch 18.11.0 (ChemAxon Ltd., http://www.chemaxon.com)
b. Estimated values using SPARC (ARChem, http://www.archemcalc.com)

2.5. Calculation of solid phase loading

Solid phase loading (ng PFAS/g GAC) of PFAS for F400 was calculated to compare it with bed volume at which half breakthrough occurs (BV_{50}).

$$\text{Solid phase loading (ng PFAS/g GAC)} = \frac{\int (C - C_0)\, dV}{M_{GAC}} = \frac{\int (C - C_0)\, d\tau \cdot BV}{M_{GAC}} \quad (1)$$

where C_0 and C indicate the PFAS concentrations in the influent and effluent (μg PFAS/L), respectively; V is the volume of filtered water (L); M_{GAC} is the mass of activated carbon (g GAC); τ is the throughput; BV is the bed volume (L).

3. Results and discussion

3.1. Impacts of Activated Carbon Diameter on PFAS Adsorption

Two similitude models are commonly employed to design RSSCTs: the constant diffusivity (CD) and proportional diffusivity (PD) models. These models are based on the dependency of

intraparticle diffusion on adsorbent size (Crittenden et al. 1991). In the case of intraparticle diffusion being independent of adsorbent size, the CD model can exhibit the exact similarity of compound breakthroughs between the RSSCT and a pilot- or full-scale fixed bed adsorber. On the other hand, the PD model maintains similarity if intraparticle diffusion is proportional to particle size. In order to scrutinize the dependency of PFAS breakthrough on particle size, three different particle sizes with the same $EBCT_{LC}$ were employed based on CD model.

As shown in Fig. 1, the breakthrough trends of PFAS for F400 coincided for the given particle sizes, which indicates that intraparticle diffusion of PFAS was independent of carbon particle size. It is noteworthy that this comparison is not conclusive for some of the favorably adsorbing PFAS such as PFOA, PFDA, PFDoDA, and PFOS since these compounds' full spectrums of breakthrough were not observed within the experimental timeframe.

[Fig. 1]

The CD model is often more beneficial over the PD model since it requires much less water, adsorbents, and time even though the PD model has often been reported to have a better prediction of pilot- or full-scale adsorption systems (Westerhoff et al. 2005). Here, the similar breakthrough trends among the different sizes of adsorbents evinces that the CD model can be used for the RSSCT for PFAS adsorption in groundwaters with a low DOC and $SUVA_{254}$ (e.g., 0.53 mg/L and 1.45 $L \cdot mg^{-1}m^{-1}$ in this study, respectively), particularly for the tested activated carbon (F400). The CD model could predict full-scale breakthroughs precisely when organic carbon content is low (Shih et al. 2003). The DOC concentrations of the tested waters were less

than 1 mg/L and such a low DOC content was attributed to the independence of intraparticle diffusion from adsorbent size. In addition, the hydraulic loading rate (HLR) can be another component influencing the selection of similitude approach (Sperlich et al. 2005). The CD model is suitable when external mass transfer controls the adsorption rate, whereas the PD model is appropriate when internal diffusion is the rate limiting step. A high HLR can enhance film transfer, thereby making internal diffusion the rate limiting step. For instance, Sperlich et al. reported better prediction with the CD model at an HLR of 0.6 $m \cdot h^{-1}$, whereas the PD model at an HLR of 11.6 $m \cdot h^{-1}$ better forecasted a large-scale column in Westerhoff et al.'s work (Sperlich et al. 2005, Westerhoff et al. 2005). Relatively low HLR in this study (3.8 $m \cdot h^{-1}$) may be another justification for the use of the CD model. It is important to note that even though the adsorbent size barely influenced the breakthrough profiles of PFAS in the given conditions of this study, PFAS breakthrough dependency on adsorbent size could still differ in a pilot- or full-scale system when dealing with a long period of operation due to pore blocking (Corwin and Summers 2010).

3.2. Roles of the Hydrophobicity of PFAS on Breakthrough Curves

Fig. 2A shows the breakthrough of the tested PFAS in the groundwater with respect to throughput in the unit of bed volume (BV, volume of filtered water divided by volume of activated carbon bed). F400 was used as the activated carbon and the EBCT for large column ($EBCT_{LC}$) was 5 min. Additionally, the tested groundwater had a low organic carbon content (DOC=0.78 mg/L) and the organic carbon had low aromaticity ($SUVA_{254}$= 1.34 $L \cdot mg^{-1}m^{-1}$). The effluent concentrations of all the tested PFAS gradually increased as throughput increased and subsequently plateaued where complete breakthrough occurred. The PFAS with shorter chains exhibited earlier breakthroughs than the ones with longer chains in the corresponding acidic

functional group (i.e., carboxylate or sulfonate). For example, PFPeA (C5) showed almost complete breakthrough at ~60,000 BVs, whereas PFOA (C8) reached complete breakthrough at a much higher BV (~250,000 BVs). Longer-chain PFAS (i.e., PFOS, C8) with sulfonate groups also showed a slower breakthrough than the shorter sulfonic PFAS (i.e., PFBS, C4). This occurs because the length of the PFAS chain influences their physico-chemical properties. Longer-chain PFAS possess greater hydrophobicities than shorter ones (Table 2). Hydrophobic interactions relate primarily to the compatibility between adsorbates and the water. Hydrophobic compounds dislike water molecules and therefore are more likely to partition into the sorbed phase. In addition, adsorbate molecules may interact with the carbon surface through non-specific dispersion forces, including forces due to the interactions with basal plane electrons and unpaired electrons located on the edges of terminated basal planes (Karanfil and Kilduff 1999). In this study, the breakthrough curve is shallower in the ascending order of hydrophobicity at the given pH (i.e., Log D_{ow}, see Table 2), confirming that hydrophobic interaction plays a crucial role in PFAS breakthrough. Further, the hydrophobicity was linearly proportional to the number of carbons (equivalently the length of PFAS) due to the rule of additivity (Fig. S4). It is important to note that no further increase in hydrophobicity of alkyl acids (without fluorine) was reported when the alkyl chain length exceeded a certain threshold (Smith and Tanford 1973). However, it was consistently observed in this study that the longer PFAS with the corresponding acidic group (carboxylate and sulfonate) showed a shallower breakthrough. Therefore, it can be inferred that increasing hydrophobicity also occurs for PFAS of chain lengths higher than 12; this is particularly true for carboxylic PFAS.

[Fig. 2]

While C/C_0 of other PFAS monotonically increased with respect to throughput, the effluent of PFBA (C4) showed higher concentrations than the influent concentration at BVs between ~20,000 and ~70,000, and subsequently decreased to values similar to the influent concentration. A similar trend, but to a less extent, was observed for PFPeA (C5). This trend was likely attributed to the displacement of adsorbed PFBA and PFPeA by dissolved organic matter (DOM) and more hydrophobic PFAS. PFBA is the most weakly adsorbing compound among the tested compounds with the lowest K_{ow} and D_{ow} values, followed by PFPeA. PFBA is expected to have the greatest mobility due to the highest molecular diffusivity (see Table 2) and surface diffusivity. As a weakly adsorbing compound, PFBA can travel faster than the other tested PFAS; hence, it can achieve its local equilibrium first like in a single component adsorption scenario (Sontheimer et al. 1988). The tested water has a low SUVA value (1.34 $L \cdot mg^{-1}m^{-1} < 2$ $L \cdot mg^{-1}m^{-1}$) and DOC content (0.53 mg/L). Immediate breakthroughs of UVA_{254} and DOC suggest that the tested water contains non-adsorbable hydrophilic fractions of DOM, which did not compete with PFAS adsorption. Interestingly, the breakthrough curve of adsorbable fractions of UV_{254}-absorbing DOM was similar to that of PFBA (see Fig. S5), inferring that the UV_{254}-absorbing DOM can directly compete with PFBA for adsorption before more hydrophobic PFAS arrive at adsorption sites. Such a DOM fraction and more hydrophobic PFAS could displace the adsorbed PFBA from the adsorptive sites. Subsequently, the desorbed PFBA was eluted together with non-adsorbed PFBA, which led to PFBA's effluent concentration exceeding its influent concentration. This phenomenon is called the "chromatographic effect" and the effluent concentration higher than the influent concentration is often referred to as an "overshoot" concentration (Hand et al. 1997). Interestingly, solid phase loading (μg PFAS/g GAC) of PFBA

was close to zero (i.e., -1.1 μg/g) (Fig. S6), which means that almost all the adsorbed PFBA was displaced by competitive adsorption and the overall amount of PFBA retained by the adsorbent is almost zero. It is noteworthy that the negative solid phase loading value was attributed to the measurement variation. In general, the chromatographic effect was more easily observed for unfavorably adsorbing compounds because the time required to achieve local equilibrium is shorter and they are also more easily displaced by DOM (Scheurer et al. 2010, Shih et al. 2005). In contrast to the observed chromatographic effect, McCleaf et al. (2017) observed the increased removal of PFDoDA (C12) and perfluorotetradecanoic acid (PFTeDA, C14) in an anion-exchange resin after 40,000 BVs whereas such an increased removal of PFAS was not observed in this study even though approximately 6 times the number of BVs (>290,000 BVs) was filtered. A sudden increase in TOC removal (around 10% to 30%) during McCleaf et al.'s experiment coincided with the increased removals of PFDoDA (C12) and PFTeDA (C14). The TOC removal increase was not discussed in their paper, but such an increased removal of hydrophobic PFAS and DOC infers that desorption of already adsorbed DOM may have occurred, which could increase the number of adsorptive sites available for the two most hydrophobic PFAS (PFDoDA and PFTeDA).

When comparing the two acidic functional groups, sulfonic PFAS had a greater hydrophobicity at the given pH (higher Log D_{ow}) than carboxylic ones with the same number of carbons even though their octanol-water partition coefficients (Log K_{ow}) are similar (Table 2); for instance, PFOS has a higher Log D_{ow} than PFOA (i.e., 3.05>1.58). An interesting finding is that the hydrophobicity of PFAS has a monotonic correlation with BV_{50} regardless of the type of acidic group (see Fig. 3). It is noted that the method for obtaining BV_{50} is described in Section S3 in the supplementary material. Here, BV_{50} was chosen as an indicator of apparent adsorption capacity

since BV_{50} can be linearly related to apparent adsorption capacity if the concentrations of target compounds are low enough (in the range of microgram per liter or below) and DOM is present (Corwin and Summers 2011). The linear relationship between the solid phase loading of PFAS and BV_{50} also supports the use of BV_{50} as an indicator of the apparent adsorption capacity (see Fig. S6). The linearity between log BV_{50} and log D_{ow} suggests that the apparent adsorption capacity of PFAS in a fixed-bed adsorber is proportional to the partition affinity of PFAS to octanol. While the other PFAS are aligned well with the fitted line, BV_{50} of PFBA (C4) was a little below the fitted line. This can be explained by PFBA experiencing breakthrough earlier than expected due to its easily desorbing nature and competitive adsorption.

[Fig. 3]

Previously, branched isomers showed less affinity for adsorption than linear forms (Eschauzier et al. 2012, McCleaf et al. 2017). In this study, it was observed that linear PFOS breakthrough was slightly shallower than branched PFOS (Fig. 4), which is consistent with previous studies. The lesser adsorption affinity of branched PFOS can be also attributed to their less hydrophobic nature. The estimated Log D_{ow} at pH 7 of branched PFOS is 2.79, whereas that of the linear form is 3.05 (see Fig. S7).

[Fig. 4]

Interestingly, when normalizing BV by BV_{50} for each PFAS, coinciding breakthrough curves were found (Fig. 2B). This suggests that the extent of the mass transfer zone development of PFAS was proportional to the apparent adsorption capacity for F400 in the given experimental conditions. Such coinciding breakthrough profiles were observed for all the tested carbons and $EBCT_{LC}$ as shown in Fig. S8. This observation may be used to estimate a breakthrough curve for a compound that was not tested, but has a known Log D_{ow}.

3.3. Impacts of Empty Bed Contact Time (EBCT)

EBCT is an important design parameter for a fixed-bed adsorber and can be controlled by changing bed height (design parameter) and/or superficial velocity (operational parameter). In this study, the adsorber bed height was altered while a fixed value of superficial velocity was employed in order to obtain three different $EBCT_{LC}$ values for F400: 5, 10 and 20 min (0.065, 0.13, and 0.26 min of $EBCT_{SC}$, respectively. See Table S5). In general, as bed length increases (or as EBCT becomes greater), the mass transfer zone gradually develops and reaches a constant width. In this study, the most weakly adsorbing PFBA exhibited a breakthrough that gradually became shallower as $EBCT_{LC}$ increased (see Fig. 5A), indicating that a greater extent of mass transfer zone development correlates with a greater EBCT. More favorably adsorbing PFPeA (C5) and PFHxA (C6) showed less prominent differences of breakthrough curve shapes among the tested EBCTs, inferring that the development of the mass transfer zone is dependent on the physico-chemical properties of PFAS. All the breakthrough curves of PFAS with respect to throughput are shown in Fig. S9. Meanwhile, the BV_{50} values among the tested EBCTs were similar to each other (Fig. 5B), which means that the apparent adsorption capacity did not change as EBCT increased. Some previous studies showed decreased adsorption capacities with increasing EBCT due to longer preloadings of DOM (Kennedy and Summers 2015, Summers et

al. 2013). DOM travels faster than hydrophobic compounds with greater adsorption affinities, which allows more time for DOM preloading with greater EBCTs (Kennedy and Summers 2015). However, no noticeable inverse relation between EBCT and PFAS adsorption capacity was found, indicating that the preloading effect of DOM was not significant enough to cause decreased adsorption capacity in the given experimental conditions. This is possibly because DOM in the tested groundwater contained low DOC with hydrophilic nature ($SUVA_{254}$=1.34 $L \cdot mg^{-1}m^{-1}$). Interestingly, the chromatographic effect becomes more pronounced as EBCT increased, particularly for PFBA (C4) and PFPeA (C5). This observation was because the longer bed allows DOM to replace a greater amount of less favorably adsorbing short-chain PFAS, which was co-eluted with their non-adsorbed fractions. The greater extent of chromatographic effect for the greater EBCTs was more clearly observed by matching the filtration time at which half breakthrough occurred (Fig. S10).

[Fig. 5]

While BV_{50} is an indicator of apparent adsorption capacity, the BV at which 10% of breakthrough occurs (BV_{10}) can be used to estimate the BV at which an early breakthrough occurs. Also, it is important to note that PFAS concentrations in effluents at BV_{10} are also close to half of the EPA health advisory level for PFOA and PFOS (half of 70 ng/L). BV_{10} exhibited a linear relation with BV_{50} with different slopes for the three EBCTs as depicted in Fig. S11A, suggesting that BV_{10} is related to the apparent adsorption capacity of F400. In addition, the slopes of BV_{10} versus BV_{50} were empirically found to be linearly proportional to the square root

of EBCT ($EBCT^{1/2}$) (Fig. S11B). Therefore, one can anticipate the slopes normalized by $EBCT^{1/2}$ to be constant as shown in Fig. S11C. This relation can be used to estimate BV_{10} using the following equation when BV_{50} is known:

$$BV_{10} = C^* \cdot BV_{50} \cdot EBCT_{LC}^{1/2} \quad \textbf{(2)}$$

where C^* is a constant value (i.e., 0.153). It is noteworthy that C^* can be expressed as a function of the inverse of BV_{50}/BV_{10} divided by $EBCT_{LC}^{1/2}$. BV_{50}/BV_{10} can be defined as the retention coefficient (RC) that accounts for competitive adsorption and pore blocking by DOM (Anumol et al. 2015). Hence, C^* is a function of the DOM effects and EBCT on PFAS breakthrough and needs to be determined for a given water quality and carbon. With a C^* of 0.153, the estimated BV_{10} of all the tested PFAS showed a less than 20% deviation from the measured values except for PFBA. Overestimation of the BV_{10} of PFBA (around 31% to 46% errors) would occur because of competitive adsorption (see Table S7 and Fig. S11D).

3.4. Effects of Surface Charge and Surface Area Distribution of Activated Carbons on PFAS Breakthrough

Fig. 6A to 6C show breakthroughs of three carboxylic PFAS (PFHxA [C6], PFHpA [C7], and PFOA [C8]) with the four activated carbons, respectively. The breakthrough curves for all PFAS are depicted in Fig. S12. Among the four tested carbons, F400 showed the slowest breakthrough profile of PFHxA (C6), followed by CMR400, HPC, and Carbsorb 40 (Fig. 6A). PFHxA breakthrough for Carbsorb 40 transpired the earliest, which can be attributed to the surface charge of the activated carbon. The pH_{PZC} of Carbsorb 40 was 7.05, indicating a net carbon surface charge of zero at the given pH (i.e., pH 7.2). The other three carbons carry net positive charges at the given pH (pH_{PZC} >9). Due to their low *p*Ka values, PFAS are negatively charged

for a wide range of pH, including neutral pH. The effects of carbon surface charges on PFAS adsorption is more clearly shown by comparing breakthrough with specific BV_{50} (see Fig. 6D). Specific BV_{50} is the BV divided by the micropore surface area and can be an indicator of apparent adsorption capacity per unit surface area of micropores. The specific BV_{50} of hydrophilic (Log D_{ow}<0) and marginally hydrophobic compounds (Log D_{ow} between 0 and 1) such as PFBA, PFPeA, PFHpA, and PFBS for Carbsorb 40, which has a net charge of zero, was lower than those of the other carbons, which had net positive charges, indicating the lower apparent adsorption capacity of Carbsorb 40 when considering micropores. While electrostatic attractions between PFAS and the three positively-charged activated carbons favor removal of PFAS, this is not expected for Carbsorb 40. Besides, while the acidic groups play the predominant roles in electronegative properties of PFAS (Erkoç and Erkoç 2001), the electronegative fluorine atoms in PFAS may also cause additional, weaker attractions to the positively charged carbon surfaces (Xiao et al. 2011).

[Fig. 6]

In addition to surface charge, micropore surface area was also imperative in determining the adsorption phenomena for hydrophilic and marginally hydrophobic PFAS. The inset of Fig. 6A shows the linear correlation between the BV_{50} of PFHxA and the micropore surface area of the three activated carbons with the same charge status (net positive charges). The three activated carbons showed similar specific BV_{50} values for a given compound (Fig. 6D), indicating that a similar amount of hydrophilic and marginally hydrophobic PFAS was adsorbed onto the unit

micropore surface area of the given amount of carbon. This also infers that micropore surfaces contain the major adsorption sites for PFAS, which may be because sorption energy is greater in micropores since multiple contact points between adsorbate and adsorbent surface are available and surface forces overlap (Karanfil and Kilduff 1999).

While charge and micropore surface area were important to determine the apparent adsorption capacity of hydrophilic and marginally hydrophobic PFAS, surface area distribution played an important role in the breakthrough of PFAS. Among the tested carbons, the RC values for PFPeA, PFBS, PFHxA, and PFOA were similar to each other except for HPC (Fig. 7 and Fig. S13). HPC has statistically higher RC values than the other carbons (Table S8), suggesting that the extent of DOM effects such as pore blocking and competitive adsorption on PFAS breakthrough is different for HPC than for other carbons. HPC has the largest mesopore surface area (336 m^2/g) and the smallest micropore surface area (451 m^2/g) among the tested carbons. Roles of pore distribution become clearer when comparing HPC with a carbon with lower mesopore surface area, but with greater micropore surface (i.e., F400 with 617 and 143 m^2/g of micro- and mesopore surface areas, respectively). Microporous F400 started breakthrough of PFHxA at a later throughput compared to mesoporous HPC while having a slightly steeper slope of the breakthrough curve (see Fig. 6A), which caused almost identical BVs at the complete breakthrough ($C/C_0=1$) even though BV_{10} and BV_{50} of F400 are higher than those of HPC. After ~120,000 BV of filtration, F400 exhibited the greater effluent concentrations of PFHpA and PFOA than HPC (Figs. 6B and 6C). This observation suggests that the role of mesoporous structure becomes increasingly important for more hydrophobic PFAS. Small organic molecules such as PFAS inherently travel through mesopores to access micropores that are the major sorption sites (Redding and Cannon 2014). It has been widely accepted that mesoporous

activated carbons suffer from less pore blocking and facilitate transport of small molecules into micropores (Li et al. 2003, Newcombe et al. 2002). DOM transporting faster than hydrophobic PFAS (e.g., UV_{254}-absorbing DOM reaching breakthrough before hydrophobic PFAS shown in Fig. S5) likely caused pore blocking prior to the hydrophobic PFAS accessing the micropores of F400. Mesoporous HPC likely suffered from less pore blocking, which facilitates hydrophobic PFAS accessing the micropores at a later BV. Furthermore, micropores narrowed by pore blockage likely excluded larger PFAS more effectively than smaller ones due to a larger minimal project diameter, a metric that evaluates molecular accessibility into pores (Table 2) (Pan et al. 2017). The lower mobility of larger molecules can be another reason for the faster breakthrough at a later throughput for microporous F400 than mesoporous HPC (Table 2). Therefore, it can be concluded that micropore surface area was imperative for breakthroughs of hydrophilic and marginally hydrophobic PFAS whereas the role of mesopores became increasingly more important for more hydrophobic PFAS eluted at a later throughput.

[Fig. 7]

4. Conclusions

The adsorption breakthrough behavior of nine perfluoroalkyl substances (PFAS) in groundwaters by fixed-bed adsorbers was studied using rapid small-scale column tests (RSSCTs) with four bituminous coal-based activated carbons (F400, Carbsorb40, HPC, and CMR400). The key findings were summarized as follows.

- Intraparticle diffusion dependency on the diameter of F400 was negligible, which suggests that the constant diffusivity model can be an appropriate similitude model in the given experimental conditions.
- Half breakthrough bed volume (BV_{50}) as an indicator of apparent adsorption capacity for F400 had a monotonic correlation with Log D_{ow} of PFAS at the given pH, indicating that hydrophobic interactions are the primary factor determining apparent adsorption capacity for F400.
- Overshoot concentrations due to the chromatographic effect were observed for hydrophilic PFAS such as PFBA (C4) and PFPeA (C5). The chromatographic effect was more prominent for the more hydrophilic PFBA.
- Longer EBCTs caused steeper PFAS breakthroughs with respect to throughput for F400 while having very similar BV_{50}. The chromatographic effect for hydrophilic PFBA and PFPeA was more pronounced for longer EBCTs due to the greater amount of desorbed PFAS coeluted with non-adsorbed PFAS.
- An empirical equation was obtained for the prediction of BV_{10} for F400 with $EBCT_{LC}$ of 5, 10, and 20 min: $BV_{10} = C^* \cdot BV_{50} \cdot EBCT_{LC}^{1/2}$.
- The activated carbons with net positive charges (F400, HPC, and CMR400) exhibited greater apparent adsorption capacity than the activated carbon with a net charge of zero (Carbsorb40).
- Micropore surface area was important for determining apparent adsorption capacity (i.e., BV_{50}) and early breakthrough (i.e., BV_{10}) for hydrophilic and marginally hydrophobic PFAS whereas mesopore surface became increasingly more important for the adsorption of more hydrophobic PFAS.

- The linear PFOS breakthrough curve was slightly steeper than that of its branched isomer due to its higher hydrophobicity.

This study was primarily designed to explain the breakthrough of PFAS in a groundwater with low organic content (< 1 mg C/L) and low $SUVA_{254}$ (<2 $L \cdot mg^{-1}m^{-1}$). It will be important to comprehensively study DOM-rich water with varying DOM characteristics like molecular weight distribution and hydrophobicity in order to understand PFAS breakthrough in a fixed-bed adsorber with various water qualities.

5. Acknowledgement

The authors would like to acknowledge the WEST center for providing the facility where the RSSCT was operated. We especially wish to acknowledge Calgon Carbon Corporation for providing the activated carbons. Mohamed Ateia and Cagri Utku Erdem at Clemson University helped with the activated carbon characterization. We also appreciate Agilent Technologies for assisting with the acquisition and maintenance of the instrumentation used in this study.

6. References

Anumol, T., Sgroi, M., Park, M., Roccaro, P. and Snyder, S.A. (2015) Predicting trace organic compound breakthrough in granular activated carbon using fluorescence and UV absorbance as surrogates. Water Research 76(0), 76-87.

Appleman, T.D., Higgins, C.P., Quiñones, O., Vanderford, B.J., Kolstad, C., Zeigler-Holady, J.C. and Dickenson, E.R.V. (2014) Treatment of poly- and perfluoroalkyl substances in U.S. full-scale water treatment systems. Water Research 51, 246-255.

Athanasaki, G., Sherrill, L. and Hristovski, K.D. (2015) The pore surface diffusion model as a tool for rapid screening of novel nanomaterial-enhanced hybrid ion-exchange media. Environmental Science: Water Research & Technology 1(4), 448-456.

Carter, K.E. and Farrell, J. (2010) Removal of Perfluorooctane and Perfluorobutane Sulfonate from Water via Carbon Adsorption and Ion Exchange. Separation Science and Technology 45(6), 762-767.

Chowdhury, Z.K. (2013) Activated carbon: solutions for improving water quality, American Water Works Association.

Corwin, C.J. and Summers, R.S. (2010) Scaling Trace Organic Contaminant Adsorption Capacity by Granular Activated Carbon. Environmental Science & Technology 44(14), 5403-5408.

Corwin, C.J. and Summers, R.S. (2011) Adsorption and desorption of trace organic contaminants from granular activated carbon adsorbers after intermittent loading and throughout backwash cycles. Water Research 45(2), 417-426.

Cousins, I.T., Vestergren, R., Wang, Z., Scheringer, M. and McLachlan, M.S. (2016) The precautionary principle and chemicals management: The example of perfluoroalkyl acids in groundwater. Environment International 94, 331-340.

Crittenden, J., Berrigan, J., Hand, D. and Lykins, B. (1987) Design of Rapid Fixed-Bed Adsorption Tests for Nonconstant Diffusivities. Journal of Environmental Engineering 113(2), 243-259.

Crittenden, J.C., Berrigan, J.K. and Hand, D.W. (1986) Design of Rapid Small-Scale Adsorption Tests for a Constant Diffusivity. Journal (Water Pollution Control Federation) 58(4), 312-319.

Crittenden, J.C., Reddy, P.S., Arora, H., Trynoski, J., Hand, D.W., Perram, D.L. and Summers, R.S. (1991) Predicting GAC Performance With Rapid Small-Scale Column Tests. Journal (American Water Works Association) 83(1), 77-87.

Dastgheib, S.A., Karanfil, T. and Cheng, W. (2004) Tailoring activated carbons for enhanced removal of natural organic matter from natural waters. Carbon 42(3), 547-557.

EPA (2019) EPA's Per- and Polyfluoroalkyl Substances (PFAS) Action Plan.

Erkoç, Ş. and Erkoç, F. (2001) Structural and electronic properties of PFOS and LiPFOS. Journal of Molecular Structure: THEOCHEM 549(3), 289-293.

Eschauzier, C., Beerendonk, E., Scholte-Veenendaal, P. and De Voogt, P. (2012) Impact of Treatment Processes on the Removal of Perfluoroalkyl Acids from the Drinking Water Production Chain. Environmental Science & Technology 46(3), 1708-1715.

Hand, D., Crittenden, J., Hokanson, D. and Bulloch, J. (1997) Predicting the performance of fixed-bed granular activated carbon adsorbers. Water Science and Technology 35(7), 235-241.

Hansen, M.C., Børresen, M.H., Schlabach, M. and Cornelissen, G. (2010) Sorption of perfluorinated compounds from contaminated water to activated carbon. Journal of Soils and Sediments 10(2), 179-185.

Hu, X.C., Andrews, D.Q., Lindstrom, A.B., Bruton, T.A., Schaider, L.A., Grandjean, P., Lohmann, R., Carignan, C.C., Blum, A., Balan, S.A., Higgins, C.P. and Sunderland, E.M. (2016) Detection of Poly- and Perfluoroalkyl Substances (PFASs) in U.S. Drinking Water Linked to Industrial Sites, Military Fire Training Areas, and Wastewater Treatment Plants. Environmental Science & Technology Letters 3(10), 344-350.

Karanfil, T. and Kilduff, J.E. (1999) Role of Granular Activated Carbon Surface Chemistry on the Adsorption of Organic Compounds. 1. Priority Pollutants. Environmental Science & Technology 33(18), 3217-3224.

Kennedy, A.M. and Summers, R.S. (2015) Effect of DOM Size on Organic Micropollutant Adsorption by GAC. Environmental Science & Technology 49(11), 6617-6624.

Li, Q., Snoeyink, V.L., Mariãas, B.J. and Campos, C. (2003) Elucidating competitive adsorption mechanisms of atrazine and NOM using model compounds. Water Research 37(4), 773-784.

Liu, C.J., Werner, D. and Bellona, C. (2019) Removal of per- and polyfluoroalkyl substances (PFASs) from contaminated groundwater using granular activated carbon: a pilot-scale study with breakthrough modeling. Environmental Science: Water Research & Technology.

McCleaf, P., Englund, S., Östlund, A., Lindegren, K., Wiberg, K. and Ahrens, L. (2017) Removal efficiency of multiple poly- and perfluoroalkyl substances (PFASs) in drinking water using granular activated carbon (GAC) and anion exchange (AE) column tests. Water Research 120, 77-87.

McNamara, J.D., Franco, R., Mimna, R. and Zappa, L. (2018) Comparison of Activated Carbons for Removal of Perfluorinated Compounds From Drinking Water. Journal - American Water Works Association 110(1), E2-E14.

Newcombe, G., Morrison, J., Hepplewhite, C. and Knappe, D.R.U. (2002) Simultaneous adsorption of MIB and NOM onto activated carbon: II. Competitive effects. Carbon 40(12), 2147-2156.

NJDEP (2018) Specific Ground Water Quality Criteria for 1,2,3-Trichloropropane (TCP) and Perfluorononanoic Acid (PFNA).

Pan, L., Takagi, Y., Matsui, Y., Matsushita, T. and Shirasaki, N. (2017) Micro-milling of spent granular activated carbon for its possible reuse as an adsorbent: Remaining capacity and characteristics. Water Research 114, 50-58.

Patterson, C., Burkhardt, J., Schupp, D., Krishnan, E.R., Dyment, S., Merritt, S., Zintek, L. and Kleinmaier, D. (2019) Effectiveness of point-of-use/point-of-entry systems to remove per- and polyfluoroalkyl substances from drinking water. AWWA Water Science 1(2).

Quiñones, O. and Snyder, S.A. (2009) Occurrence of Perfluoroalkyl Carboxylates and Sulfonates in Drinking Water Utilities and Related Waters from the United States. Environmental Science & Technology 43(24), 9089-9095.

Redding, A.M. and Cannon, F.S. (2014) The role of mesopores in MTBE removal with granular activated carbon. Water Research 56, 214-224.

Scheurer, M., Storck, F.R., Brauch, H.-J. and Lange, F.T. (2010) Performance of conventional multi-barrier drinking water treatment plants for the removal of four artificial sweeteners. Water Research 44(12), 3573-3584.

Senevirathna, S.T.M.L.D., Tanaka, S., Fujii, S., Kunacheva, C., Harada, H., Shivakoti, B.R. and Okamoto, R. (2010) A comparative study of adsorption of perfluorooctane sulfonate (PFOS) onto granular activated carbon, ion-exchange polymers and non-ion-exchange polymers. Chemosphere 80(6), 647-651.

Shih, T., Wangpaichitr, M. and Suffet, M. (2005) Performance and Cost Evaluations of Synthetic Resin Technology for the Removal of Methyl Tert-Butyl Ether from Drinking Water. Journal of Environmental Engineering 131(3), 450-460.

Shih, T.C., Wangpaichitr, M. and Suffet, M. (2003) Evaluation of granular activated carbon technology for the removal of methyl tertiary butyl ether (MTBE) from drinking water. Water Research 37(2), 375-385.

Siriwardena, D.P., Crimi, M., Holsen, T.M., Bellona, C., Divine, C. and Dickenson, E. (2019) Influence of groundwater conditions and co-contaminants on sorption of perfluoroalkyl compounds on granular activated carbon. Remediation Journal 29(3), 5-15.

Smith, R. and Tanford, C. (1973) Hydrophobicity of long chain n-alkyl carboxylic acids, as measured by their distribution between heptane and aqueous solutions. Proceedings of the National Academy of Sciences 70(2), 289-293.

Sontheimer, H., Crittenden, J.C. and Summers, R.S. (1988) Activated carbon for water treatment.

Sperlich, A., Werner, A., Genz, A., Amy, G., Worch, E. and Jekel, M. (2005) Breakthrough behavior of granular ferric hydroxide (GFH) fixed-bed adsorption filters: modeling and experimental approaches. Water Research 39(6), 1190-1198.

Summers, R.S., Kim, S.M., Shimabuku, K., Chae, S.-H. and Corwin, C.J. (2013) Granular activated carbon adsorption of MIB in the presence of dissolved organic matter. Water Research 47(10), 3507-3513.

Sun, M., Arevalo, E., Strynar, M., Lindstrom, A., Richardson, M., Kearns, B., Pickett, A., Smith, C. and Knappe, D.R.U. (2016) Legacy and Emerging Perfluoroalkyl Substances Are Important Drinking Water Contaminants in the Cape Fear River Watershed of North Carolina. Environmental Science & Technology Letters 3(12), 415-419.

SWRCB (2019) Perfluorooctanoic acid (PFOA) and Perfluorooctanesulfonic acid (PFOS).

Westerhoff, P., Highfield, D., Badruzzaman, M. and Yoon, Y. (2005) Rapid Small-Scale Column Tests for Arsenate Removal in Iron Oxide Packed Bed Columns. Journal of Environmental Engineering 131(2), 262-271.

Worch, E. (2008) Fixed-bed adsorption in drinking water treatment: a critical review on models and parameter estimation. Journal of Water Supply: Research and Technology-AQUA 57(3), 171-183.

Xiao, F., Zhang, X., Penn, L., Gulliver, J.S. and Simcik, M.F. (2011) Effects of Monovalent Cations on the Competitive Adsorption of Perfluoroalkyl Acids by Kaolinite: Experimental Studies and Modeling. Environmental Science & Technology 45(23), 10028-10035.

Xiao, X., Ulrich, B.A., Chen, B. and Higgins, C.P. (2017) Sorption of Poly- and Perfluoroalkyl Substances (PFASs) Relevant to Aqueous Film-Forming Foam (AFFF)-Impacted Groundwater by Biochars and Activated Carbon. Environmental Science & Technology 51(11), 6342-6351.

Yu, J., Lv, L., Lan, P., Zhang, S., Pan, B. and Zhang, W. (2012) Effect of effluent organic matter on the adsorption of perfluorinated compounds onto activated carbon. Journal of Hazardous Materials 225–226, 99-106.

Yu, Q., Zhang, R., Deng, S., Huang, J. and Yu, G. (2009) Sorption of perfluorooctane sulfonate and perfluorooctanoate on activated carbons and resin: Kinetic and isotherm study. Water Research 43(4), 1150-1158.

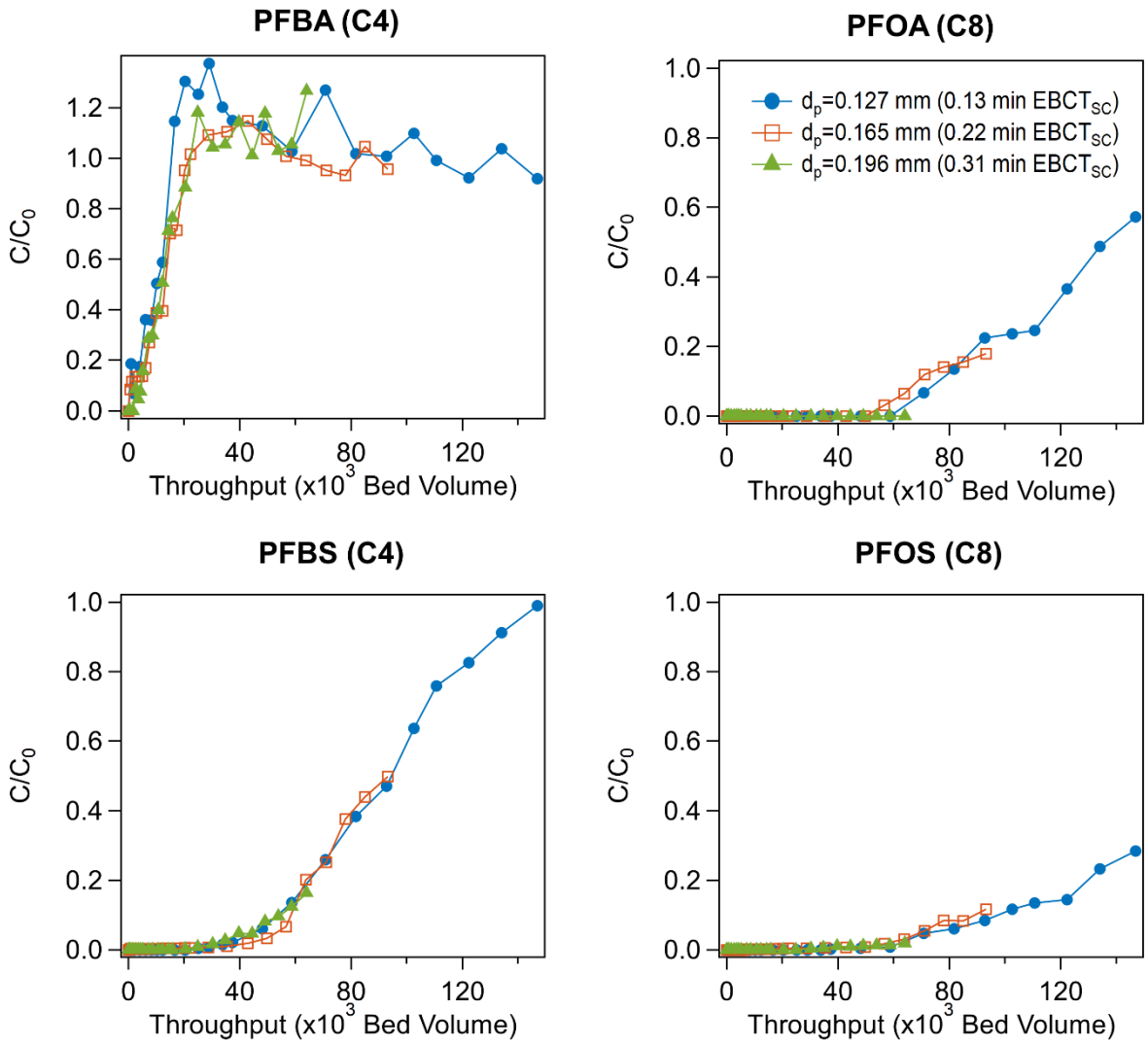

Fig. 1. Breakthrough curves of two carboxylic PFAS (PFBA and PFOA) and two sulfonic PFAS (PFBS and PFOS) with respect to different mean particle diameter (d_p). DOC concentration was 0.53 mg/L. F400 was used as an adsorbent and 10 min of $EBCT_{LC}$ was employed. Reynolds number (Re) values for 0.13, 0.22, and 0.31 min of $EBCT_{SC}$ were 0.30, 0.39, and 0.46, respectively.

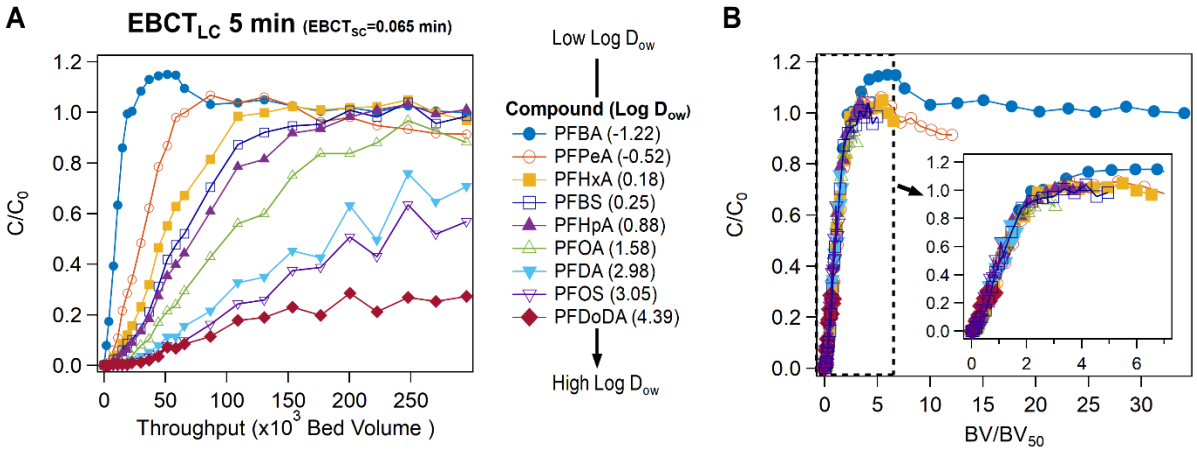

Fig. 2. Breakthrough curves of PFAS with respect to throughput in the unit of bed volume (BV) (A) and with respect to throughput normalized by half breakthrough BV (BV/BV_{50}) (B). DOC concentration of the feed water was 0.78 mg/L. F400 was used as an adsorbent and 5 min of $EBCT_{LC}$ (0.065 min of $EBCT_{SC}$) was employed. Re was 0.30.

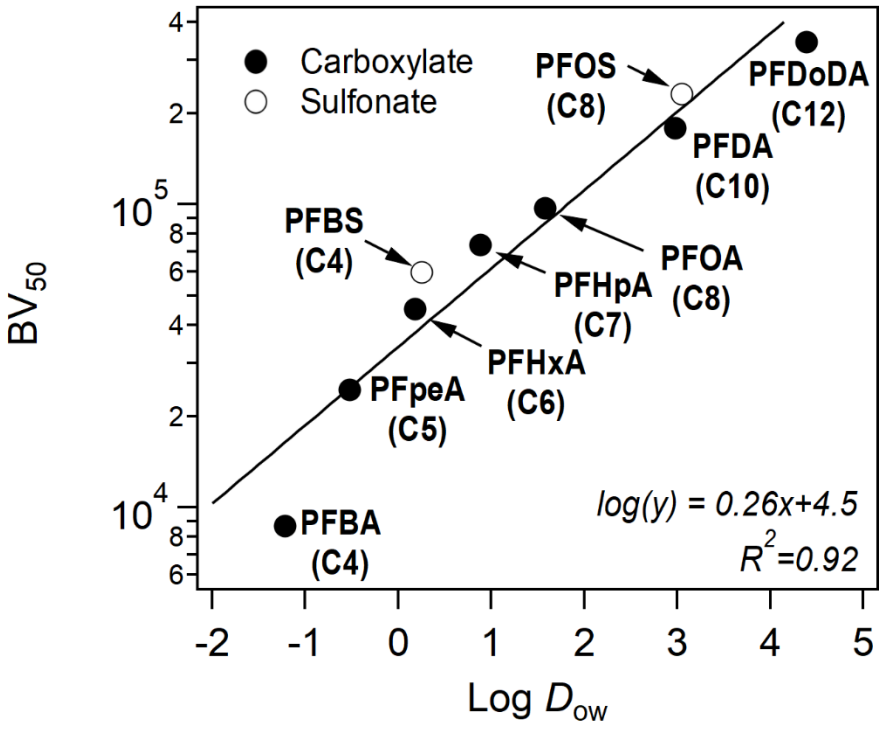

Fig. 3. Half breakthrough bed volume (BV_{50}) of PFAS versus Log D_{ow}. F400 was used as an adsorbent and 5 min of $EBCT_{LC}$ (0.065 min of $EBCT_{SC}$) was employed. Re was 0.30.

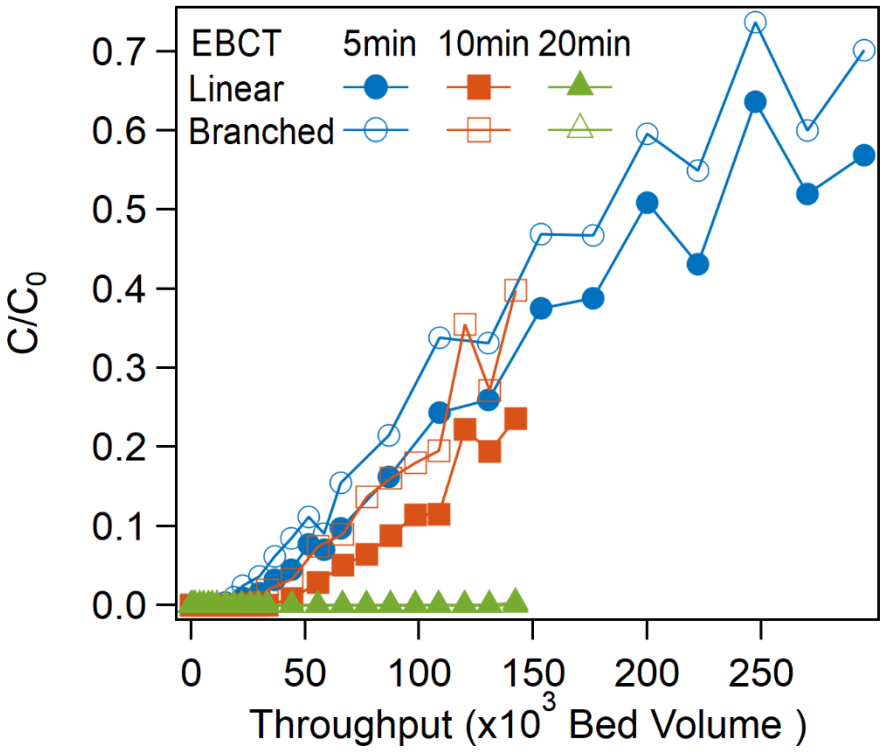

Fig. 4. Breakthrough curves of linear and branched PFOS. The DOC concentration was 0.78 mg/L. F400 was used as an adsorbent. Re was 0.30.

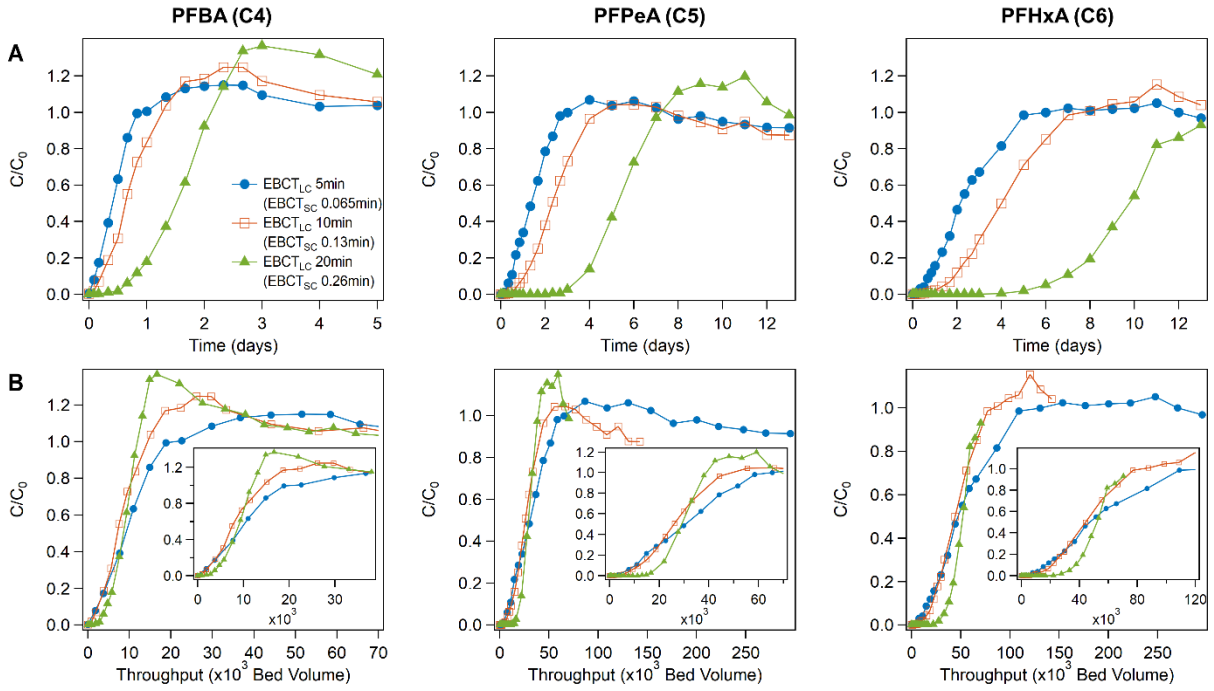

Fig. 5. Breakthrough curves of PFBA (C4), PFPeA (C5), and PFHxA (C6) with respect to filtration time (A) and throughput (B) for 5, 10, and 20 min of $EBCT_{LC}$. DOC concentration of the feed water was 0.78 mg/L. F400 was used as an adsorbent. Re was 0.30.

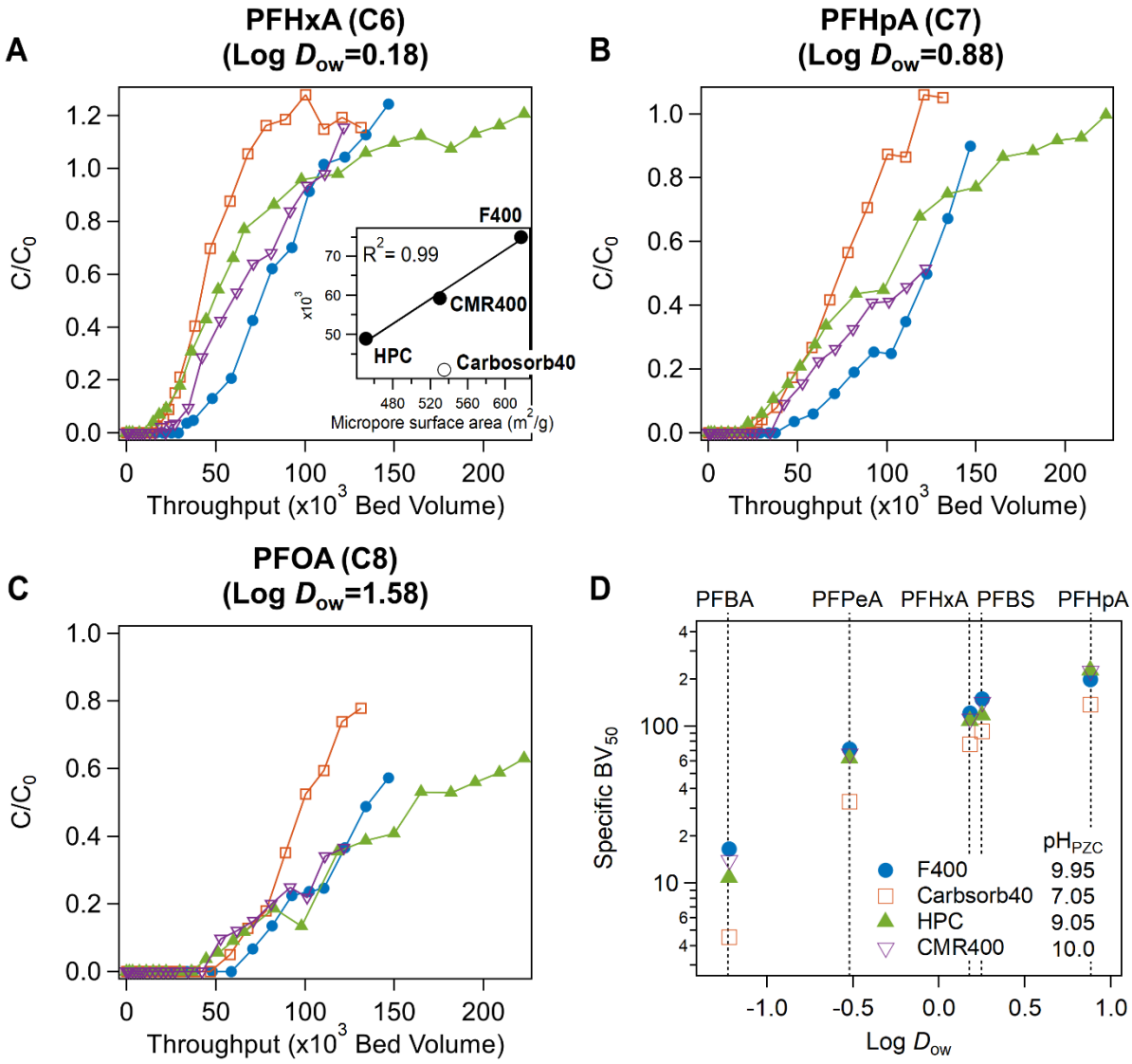

Fig. 6. Breakthrough curves of PFHxA (A), PFHpA (B), and PFOA (C). The specific BV_{50} values with respect to Log D_{ow} for PFAS that could obtain BV_{50} values for the all four activated carbons are shown in (D). The inset of (A) is the plot of BV_{50} versus micropore surface area. The linear regression of three carbons with net positive charges (solid black circles) was presented. The DOC concentration of the feed water was 0.53 mg/L. Ten min of $EBCT_{LC}$ was employed and corresponding $EBCT_{SC}$ values for each activated carbon are shown in Table S6.

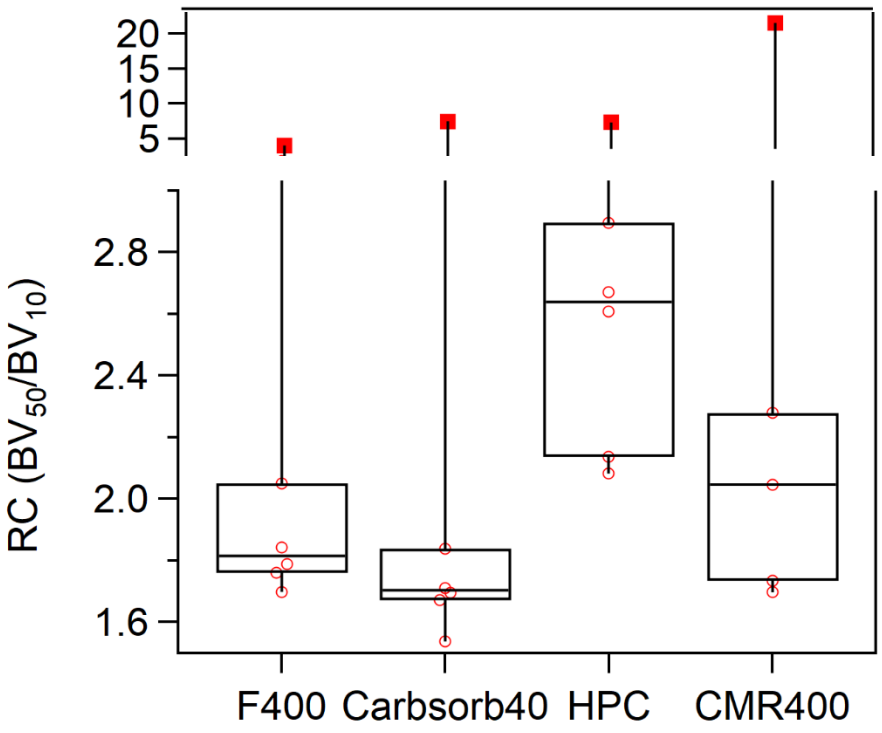

Fig. 7. Box plot of the retention coefficients (RCs) of the tested activated carbons for PFBA, PFPeA, PFHxA, PFHpA, PFOA, and PFBS. Solid red symbols are outliers that are the RCs of PFBA. BV_{10}/BV_{50} distribution of HPC for PFPeA, PFHxA, PFHpA, PFOA, and PFBS was statistically different from the other carbons based on t-test (see Table S8).

Table 1 Mean particle diameter (MPD), Brunauer–Emmett–Teller (BET) surface distribution, pore volume distribution, and pH at point of zero charge (pH_{PZC}) of the tested activated carbons

Adsorbent	Mean particle diameter (mm)[a]	BET surface area (m^2/g)	BET surface area distribution (m^2/g)			Total pore Volume (cm^3/g)	Pore volume distribution (cm^3/g)			pH_{PZC}
			< 2 nm	2 - 50 nm	> 50 nm		< 2 nm	2 - 50 nm	> 50 nm	
F400	1.122	769	617	143	9	0.41	0.33	0.08	0.00	9.95
Carbsorb40	1.413	755	535	219	1	0.40	0.28	0.12	0.00	7.05
HPC 8x30	1.005	788	451	336	1	0.31	0.18	0.13	0.00	9.05
CMR400[b]	1.015	767	530	224	13	0.41	0.29	0.12	0.01	10.00

a. MPD values were provided by Calgon Carbon Corporation

b. custom municipal reactivated carbon that underwent a steam reactivation (McNamara et al. 2018)

Table 2 Names, abbreviations, number of carbons, structures, octanol-water partition coefficient (Log K_{ow}), octanol-water partition coefficient at pH 7 (Log D_{ow} at pH 7), bulk diffusivity (D), and minimal/maximal projection diameter values of the tested PFAS

Compound, Number of carbons	Structure	Log K_{ow}[a]	Log D_{ow} at pH7[a]	D[b] (cm^2/sec)	Minimal/ maximal projection diameter (nm)[a]
Perfluorobutanoic acid (PFBA), C4	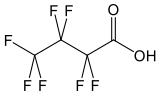	2.31	-1.22	7.89×10^{-6}	0.64 / 0.92
Perfluoropentanoic acid (PFpeA), C5	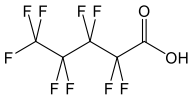	3.01	-0.52	7.19×10^{-6}	0.66 / 1.0
Perfluorohexanoic acid (PFHxA), C6	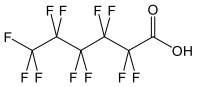	3.71	0.18	6.58×10^{-6}	0.72 / 1.1
Perfluoroheptanoic acid (PFHpA), C7	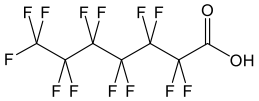	4.41	0.88	6.06×10^{-6}	0.82 / 1.2
Perfluorooctanoic acid (PFOA), C8	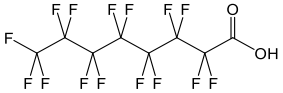	5.11	1.58	5.63×10^{-6}	0.78 / 1.3
Perfluorodecanoic acid (PFDA), C10	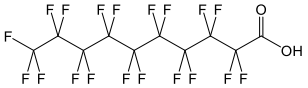	6.51	2.98	4.93×10^{-6}	0.78 / 1.6
Perfluorododecanoic acid (PFDoDA), C12	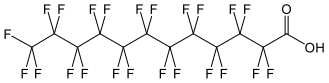	7.92	4.39	4.40×10^{-6}	0.80 / 1.8
Perfluorobutanesulfonic acid (PFBS), C4	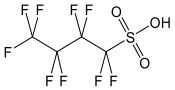	2.63	0.25	7.15×10^{-6}	0.70 / 1.0
Perfluorooctanesulfonic acid (PFOS), C8	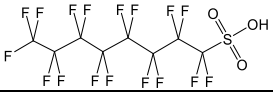	5.43	3.05	5.21×10^{-6}	0.80 / 1.3

a. Estimated data obtained using MarvinSketch 18.11.0 (ChemAxon Ltd., http://www.chemaxon.com)
b. Estimated values using SPARC (ARChem, http://www.archemcalc.com)

Adsorption of Perfluoroalkyl Substances (PFAS) in Groundwater by Granular Activated Carbons: Roles of Hydrophobicity of PFAS and Carbon Characteristics

Minkyu Park[a,*], Shimin Wu[a,b], Israel J. Lopez[a], Joseph Y. Chang[a], Tanju Karanfil[c], and Shane A. Snyder[a,d,†*]

a. Department of Chemical & Environmental Engineering, University of Arizona, 1133 E James E Rogers Way, Harshbarger 108, Tucson, AZ 85721-0011, USA
b. IER Environmental Protection Engineering Technology Co., Ltd., Shenzhen 518071, China
c. Department of Environmental Engineering and Earth Sciences, Clemson University, Anderson, SC 29625, USA
d. Nanyang Technological University, Nanyang Environment & Water Research Institute (NEWRI), Singapore 637141

Supplementary Material

† Corresponding author: minkyupark@email.arizona.edu
†* Corresponding author: snyders2@email.arizona.edu

Table of Contents

S1. Chemical vendors and purities for the tested PFAS

The PFAS chemical standards were purchased from various vendors. Their purity and CAS numbers are summarized in Table S1

Table S1 CAS numbers, vendors, and purities of the tested PFAS

Compound, Number of carbons	CAS No.	Vendor	Purity
Perfluorobutanoic acid (PFBA), C4	375-22-4	Sigma Aldrich	≥98%
Perfluoro-*n*-pentanoic acid (PFpeA), C5	2706-90-3	Sigma Aldrich	97%
Perfluorohexanoic acid (PFHxA), C6	307-24-4	Sigma Aldrich	≥97%
Perfluoroheptanoic acid (PFHpA), C7	375-85-9	Sigma Aldrich	99%
Perfluorooctanoic acid (PFOA), C8	335-67-1	Sigma Aldrich	95%
Perfluorodecanoic acid (PFDA), C10	335-76-2	Alfa Aesar	97%
Perfluorododecanoic acid (PFDoDA), C12	307-55-1	Matrix Scientific	96%
Perfluorobutanesulfonic acid (PFBS), C4	375-73-5	Sigma Aldrich	97%
Perfluorooctanesulfonic acid (PFOS), C8	1763-23-1	Sigma Aldrich	≥98%

Perfluoro-*n*-[$^{13}C_4$]butanoic acid (PFBA-$^{13}C_4$)	N/A	Wellington Laboratories Inc.	50 μg/ml in MeOH
Perfluoro-*n*-[1,2-$^{13}C_2$]hexanoic acid (PFHxA-$^{13}C_2$)	N/A	Wellington Laboratories Inc.	50 μg/ml in MeOH
Perfluoro-*n*-[1,2,3,4-$^{13}C_4$]octanoic acid (PFOA-$^{13}C_4$)	N/A	Wellington Laboratories Inc.	50 μg/ml in MeOH
Sodium perfluoro-1-[1,2,3,4-$^{13}C_4$]octanesulfonate (PFOS-$^{13}C_4$)	N/A	Wellington Laboratories Inc.	50 μg/ml in MeOH
Perfluoro-*n*-[1,2-$^{13}C_2$]decanoic acid (PFDA-$^{13}C_2$)	N/A	Wellington Laboratories Inc.	50 μg/ml in MeOH

S2. Analytical methods for the detection of PFAS

The liquid chromatography (LC) separation was conducted using an Agilent 1290 ultra high-performance LC (UHPLC) system (Agilent Technologies, Palo Alto, CA), with an Agilent ZORBAX RRHD Eclipse Plus C18 column (2.1 × 100 mm, 1.8 μm particle size). The column temperature was maintained at 30 °C. Ultrapure water containing 5 mM ammonium acetate (A) and methanol (B) was used as a mobile phase with a constant flow rate of 0.4 mL/min. The gradient was as follows: 5% B was initially applied and linearly increased to 60% in 2 min, followed by a linear increase to 100% in the next 8 min. B was held at 100% for 2 min and returned to 5% for a 3.0-min post-run column equilibration.

Mass spectrometric detection was performed using an Agilent 6490 triple quadrupole mass spectrometer (Agilent Technologies, Palo Alto, CA) equipped with the Jet Stream dual

electrospray ionization (ESI) source and iFunnel technology. The instrument was operated using an electrospray ionization source (ESI) in negative mode, with optimized parameters as follows: gas temperature, 250 ℃; gas flow, 14 L/min; sheath gas temperature, 375 ℃; sheath gas flow, 12 L/min; nebulizer, 45 psi; capillary voltage, 3500 V; fragmentor, 380 V. The optimized MRM transition parameters for the analytes are listed in Table S2. Note that the product ions refer to quantifiers and no qualifiers were employed. The LC-MS/MS chromatogram of target PFAS is displayed in Fig. S1.

All analytes were calibrated internally using linear regression with 1/*x* weighting based on the relative response factors (RRFs) for the analytes and their corresponding isotopically labelled standards (ILSs) (Table S2). Calibration curves of at least nine points were constructed over the concentration range of 1.0–500 ng/L for each analyte with 250 ng/L of ILSs. Data acquisition and analysis were performed using the Agilent MassHunter Workstation Software (Ver. 6.00). The minimum reporting limits (MRLs), which was defined as the concentration of the second lowest calibration curve point of each tested PFAS (Vanderford et al. 2003), are also showed in Table S2.

Table S2 Optimized MRM conditions and MRLs of target PFAS.

Compound	RT (min)	ILSS	Prec Ion	Prod Ion	CE (V)	ESI	MRL (ng/L)
PFBA	3.75	PFBA-$^{13}C_4$	213.0	168.9	4	Neg	2.0
PFPeA	4.43	PFHxA-$^{13}C_2$	263.0	218.9	8	Neg	2.0
PFBS	4.52	PFHxA-$^{13}C_2$	298.9	79.8	44	Neg	1.0
PFHxA	5.00	PFHxA-$^{13}C_2$	313.0	268.9	4	Neg	1.0
PFHpA	5.64	PFHxA-$^{13}C_2$	363.0	318.9	8	Neg	1.0
PFOA	6.32	PFOA-$^{13}C_4$	413.0	368.9	8	Neg	1.0
PFOS	6.98	PFOS-$^{13}C_4$	498.9	79.9	60	Neg	1.0
PFDA	7.65	PFDA-$^{13}C_2$	513.0	469.0	8	Neg	2.0
PFDoDA	8.73	PFDA-$^{13}C_2$	613.0	569.0	12	Neg	1.0
Branched PFOS	6.79	PFOS-$^{13}C_4$	498.9	79.9	60	Neg	1.0

ILSs							
PFBA-$^{13}C_4$	3.75	–	217.0	171.9	4	Neg	–
PFHxA-$^{13}C_2$	5.00	–	315.0	270.1	4	Neg	–
PFOA-$^{13}C_4$	6.33	–	416.9	372.0	8	Neg	–
PFOS-$^{13}C_4$	6.98	–	502.9	79.9	50	Neg	–
PFDA-$^{13}C_2$	7.65	–	515.0	469.8	8	Neg	–

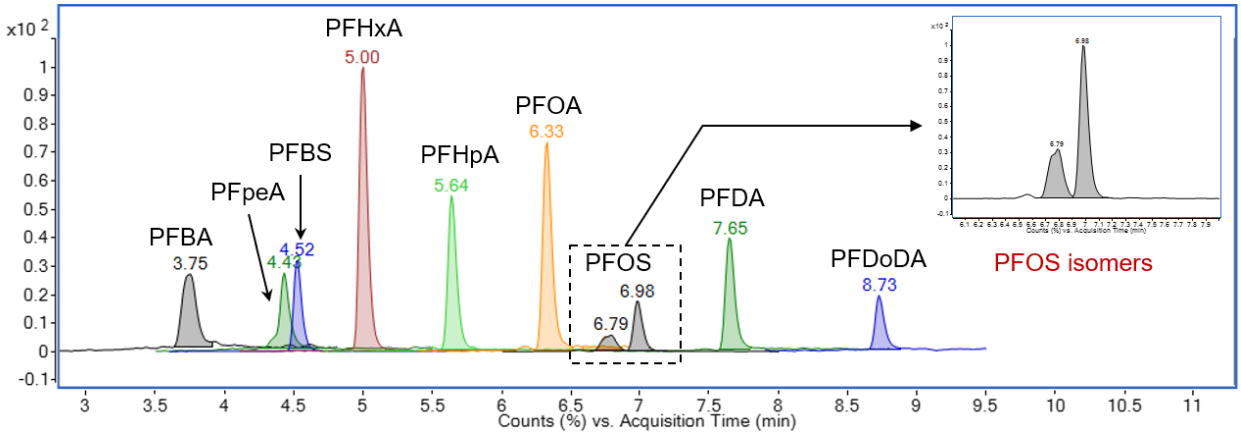

Fig. S1 LC-MS/MS chromatogram of target PFAS in ultrapure water at 5 ng/L.

S3. Interpolation and extrapolation for obtaining BV_{50} and BV_{10}

In this study, BV_{50} was chosen as an indicator of apparent adsorption capacity. Further, BV_{10} was also used to understand PFAS breakthroughs (Section 3.3 and 3.4). Except for Section 3.2., linear interpolation between the two closest data points to obtain BV_{50} and BV_{10}. In Section 3.2., dispersed flow, local equilibrium model (DFLEM) was used to inter- and extrapolate breakthrough data points in order to assess the relation between BV_{50} and Log D_{ow} for all the tested PFAS including those that did not reach to half breakthrough (i.e.., PFDoDA). DFLEM was derived with the assumptions that mass transfer resistance is negligible and local equilibrium between stationary and mobile phases is achieved. When Peclet number (Pe) is sufficiently large, the following equation can be achieved (Hashimoto et al. 1964, Hutzler et al. 1986).

$$\frac{C}{C_0} = \frac{1}{2} erfc\left(\sqrt{Pe}\frac{1-\tau}{\sqrt{\tau}}\right) + \frac{1}{2\sqrt{\pi}}\sqrt{\frac{\tau}{Pe}}\exp\left(-Pe\frac{(1-\tau)^2}{\tau}\right)\frac{\tau^2+4\tau-1}{(\tau+1)^3}$$

where τ refers to the throughput. It is noteworthy that the DFLEM model does not have any physical interpretation in this study since physical parameters were estimated based on the goodness of fit. In addition, the estimated Pe values were not sufficiently large (the estimated Pe<<40. See Table S3). Therefore, the model was used to interpolate and extrapolate the data in order to find BV_{50} for Section 3.2, and physical interpretation is not adequate.

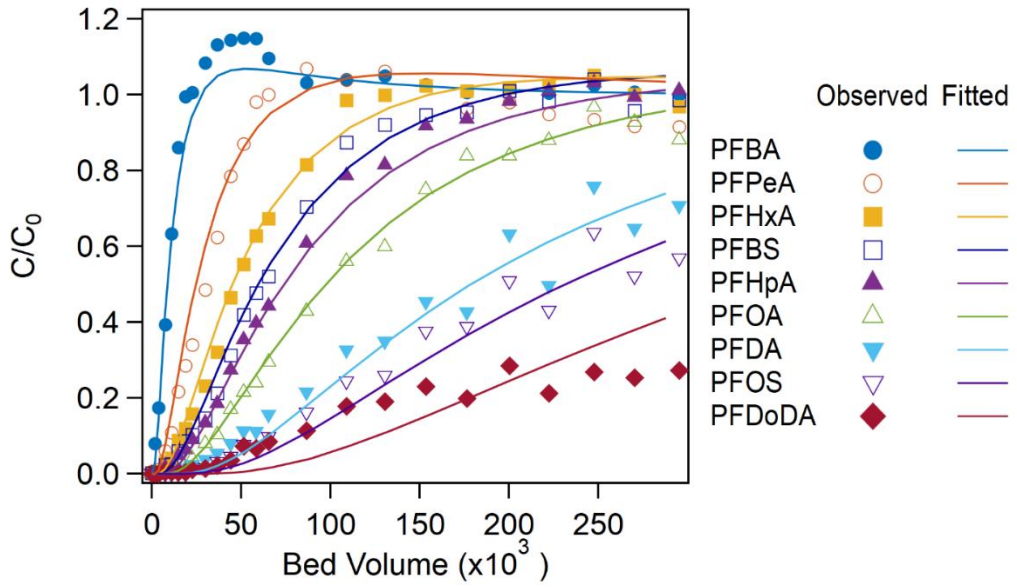

Fig. S2. Breakthrough curves of PFAS shown in Fig. 2 of the main text. The symbols refer to the observed data and the solid lines indicate the fitted data that were obtained using the dispersed flow, local equilibrium model (DFLEM).

Table S3 shows the goodness-of-fit (R^2) and estimated Pe values. While the most compounds have high R^2 values (>0.95) The most hydrophobic PFDoDA has relatively lower R^2 value (i.e., 0.80).

Table S3. The goodness-of-fit values of DFLEM fitting and the estimated Pe values.

	PFBA	PFPeA	PFHxA	PFBS	PFHpA	PFOA	PFDA	PFOS	PFDoDA
R^2	0.98	0.97	0.99	0.99	0.99	0.99	0.97	0.96	0.80
Pe	0.14	0.15	0.17	0.15	0.18	0.20	0.22	0.21	0.25

S4. Supplementary tables

Table S4 Scale-down properties for modeling of RSSCTs for Section 3.1. LC and SC indicate fictive large column and actual small column, respectively. The mesh size of #100/#140, #80/#100, and #70/#80 was used to achieve MPD_{SC} of 0.128, 0.165, and 0.196 mm, respectively. The water used was from the second sampling campaign (DOC=0.53 mg/L and $SUVA_{254}$] of 1.45 $L \cdot mg^{-1}m^{-1}$). Reynolds numbers (Re) were calculated using the equation that $Re=2\rho R v_s/\mu$ where ρ is the water viscosity at 25°C; R is the radius of activated carbon; v_s is the specific discharge (i.e., the flowrate divided by the area of a column); μ is the viscosity of water at 25°C.

Activated carbon	F400	F400	F400
$EBCT_{LC}$ (min)	10	10	10
$EBCT_{SC}$ (min)	0.130	0.215	0.305
MPD_{LC} (mm)	1.122	1.122	1.122
MPD_{SC} (mm)	0.128	0.165	0.196
Bed diameter (cm)	1	1	1
Bed height (cm)	0.8	1.4	1.9
Bed volume $_{SC}$ (cm^3)	0.651	1.075	1.526
Flow rate $_{SC}$ (mL/min)	5	5	5
Hydraulic loading (m/hr)	3.8	3.8	3.8
Reynolds number (-)	0.30	0.39	0.46

Table S5 Scale-down properties for modeling of RSSCTs for Section 3.2 and 3.3. Mean particle diameter (MPD) values for LC were provided by the vendor (i.e., Calgon Carbon). The mesh

size of #100 and #140 was used. The water used was from the first sampling campaign (DOC=0.78 mg/L and $SUVA_{254}$] of 1.34 $L \cdot mg^{-1}m^{-1}$).

Activated carbon	F400	F400	F400
$EBCT_{LC}$ (min)	5	10	20
$EBCT_{SC}$ (min)	0.065	0.130	0.260
MPD_{LC} (mm)	1.122	1.122	1.122
MPD_{SC} (mm)	0.128	0.128	0.128
Bed diameter (cm)	1	1	1
Bed height (cm)	0.4	0.8	1.7
Bed volume $_{SC}$ (cm^3)	0.325	0.651	1.301
Flow rate $_{SC}$ (mL/min)	5	5	5
Hydraulic loading (m/hr)	3.8	3.8	3.8
Reynolds number (-)	0.30	0.30	0.30

Table S6 Scale-down properties for modeling of RSSCTs for Section 3.4. The mesh size of #100 and #140 was used. The water used was from the second sampling campaign (DOC=0.53 mg/L and $SUVA_{254}$] of 1.45 $L \cdot mg^{-1}m^{-1}$).

Activated carbon	F400	Carbsorb 40	HPC 8x40	CMR400
$EBCT_{LC}$ (min)	10	10	10	10
$EBCT_{SC}$ (min)	0.130	0.162	0.082	0.159
MPD_{LC} (mm)	1.122	1.005	1.413	1.015

MPD_{SC} (mm)	0.128	0.128	0.128	0.128
Bed diameter (cm)	1	1	1	1
Bed height (cm)	0.8	1.0	0.5	1.0
Bed volume $_{SC}$ (cm^3)	0.651	0.811	0.410	0.795
Flow rate $_{SC}$ (mL/min)	5	5	5	5
Hydraulic loading (m/hr)	3.8	3.8	3.8	3.8
Reynolds number (-)	0.30	0.30	0.30	0.30

Table S7 Percent error values of estimated BV_{10}.

$EBCT_{LC}$	PFBA	PFPeA	PFHxA	PFBS	PFHpA	PFOA	PFDA	PFOS	PFDoDA
5min	34.7	-19.2	-5.8	-7.3	4.5	-7.0	15.0	17.4	N/A
10min	46.2	5.0	2.1	2.1	5.1	-4.9	1.0	4.9	N/A
20min	31.3	-1.2	-4.3	-8.8	-8.7	N/A	N/A	N/A	N/A

N/A indicates Not Available.

Table S8 *p*-values of BV_{50}/BV_{10} values between two different activated carbons. Two-sample equal variance t-test with two-tailed distribution was conducted in Microsoft Excel. *p*-values lower than 0.05 were highlighted in color.

Carbon	**F400**	**Carbsorb40**	**HPC**	**CMR400**
F400	1.00	0.11	0.00	0.45
Carbsorb40	0.11	1.00	0.00	0.10
HPC	0.00	0.00	1.00	0.04
CMR400	0.45	0.10	0.04	1.00

S5. Supplementary figures

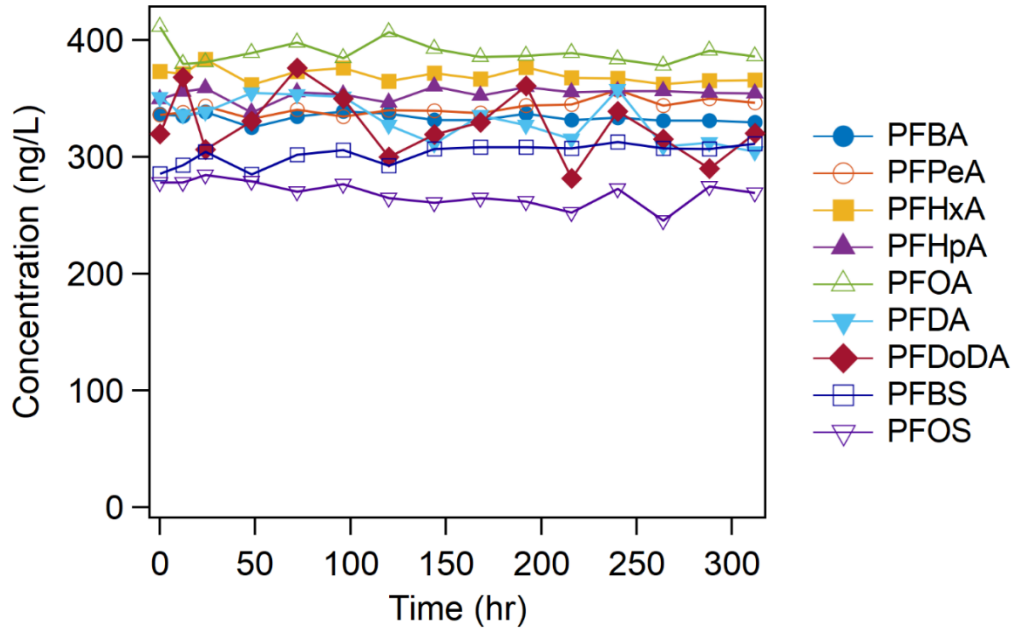

Fig. S3. The concentrations of PFAS in the feed water tank over the sampling period of the first campaign. No noticeable degradation of PFAS over the sampling period were observed.

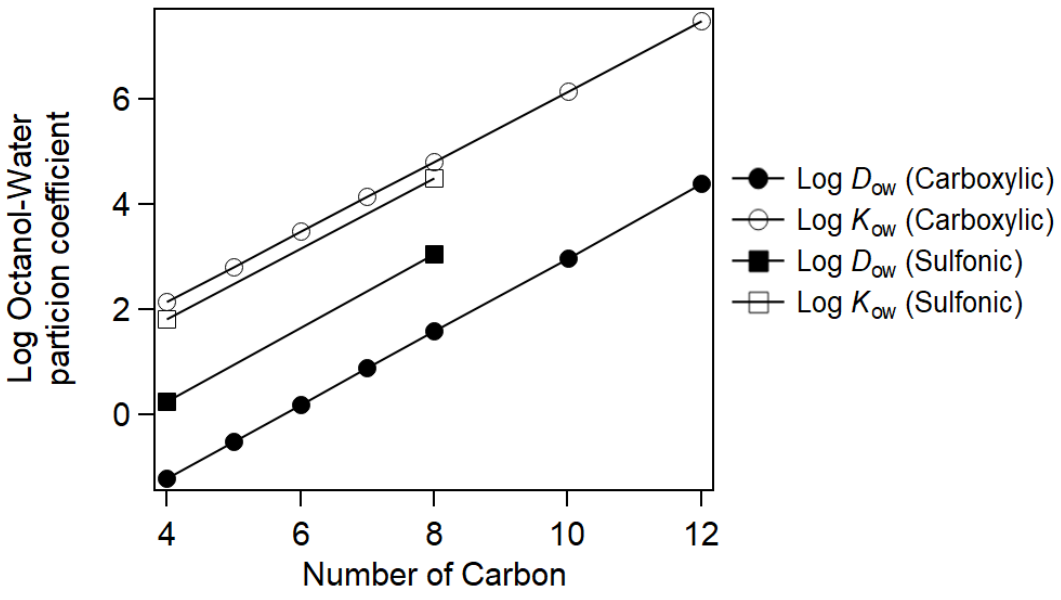

Fig. S4. Estimated log octanol-water partition coefficients of the tested PFAS with respect to the number of carbon.

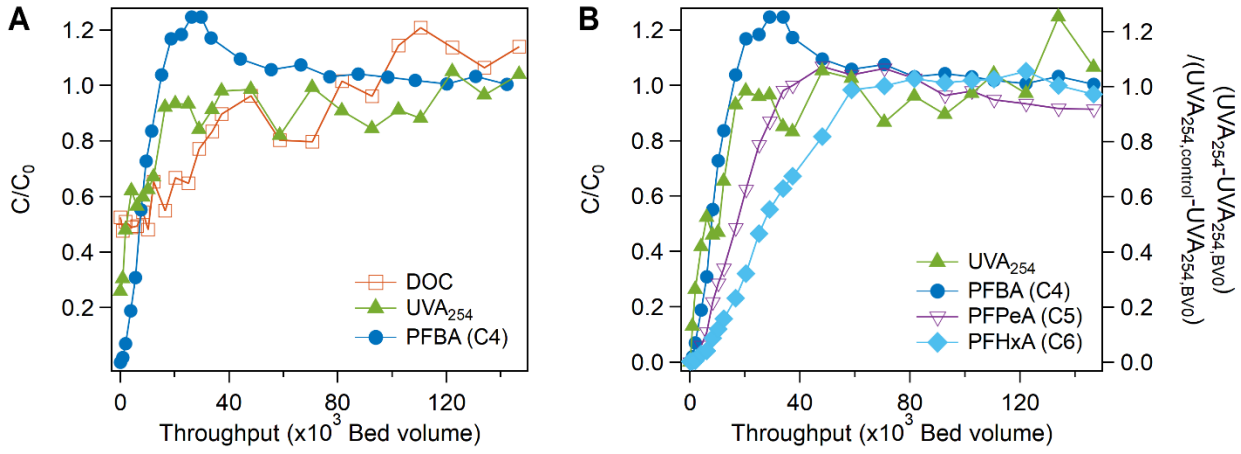

Fig. S5. Breakthrough curves of DOC, UVA_{254}, and PFBA for F400 carbon (A). Since it was presumed that the UV-absorbing DOC fraction that initially breakthroughed (i.e., $UVA_{254,BV0}$, referring to UVA_{254} of effluents at zero bed volume) is non-adsorbable, the breakthrough of adsorbable fraction (i.e., $[UVA_{254}\text{-}UVA_{254,BV0}]/[UVA_{254,control}\text{-}UVA_{254,BV0}]$) was shown along with the three selected PFAS in (B) where UVA_{254} and $UVA_{254,control}$ indicate UVA_{254} of the effluents and influents (controls) at a given time, respectively. F400 was used as an adsorbent and 5 min of $EBCT_{LC}$ (0.065 min of $EBCT_{SC}$) was employed.

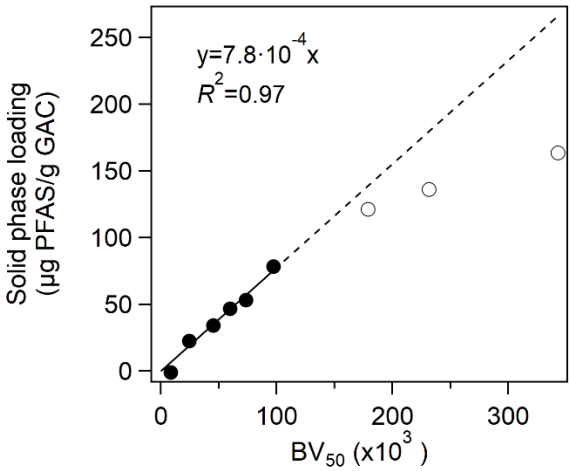

70

71 **Fig. S6**. Solid phase loading of PFAS (µg PFAS/g GAC) for F400 with 5 min of $EBCT_{LC}$ (0.065
72 min of $EBCT_{SC}$). Solid symbols are the solid phase loadings of PFAS exhibiting full
73 breakthrough profiles (i.e., reached to ~1 of C/C_0) whereas open symbols are those that did not
74 reach to C/C_0 of 1. Linear regression was conducted for the solid symbols. PFAS with the open
75 symbols (i.e., PFDA, PFDoDA, and PFOS) were below the fitted line because full loading could
76 not be achieved within the experimental timeframe.

77

Linear PFOS

$Log\ K_{ow} = 5.43$
$Log\ D_{ow} = 3.05$

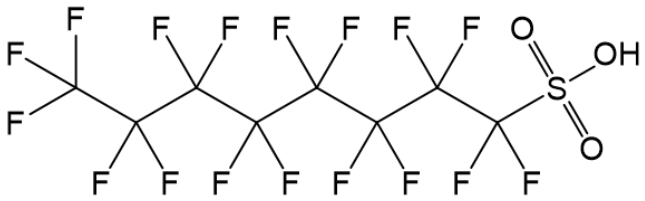

Branched PFOS

$Log\ K_{ow} = 5.17$
$Log\ D_{ow} = 2.79$

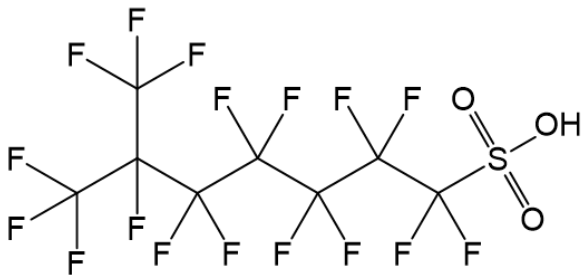

78

Fig. S7. Chemical structures and hydrophobicities of linear and branched PFOS. The log K_{ow} and D_{ow} were estimated using MarvinSketch 18.11.0 (ChemAxon Ltd.).

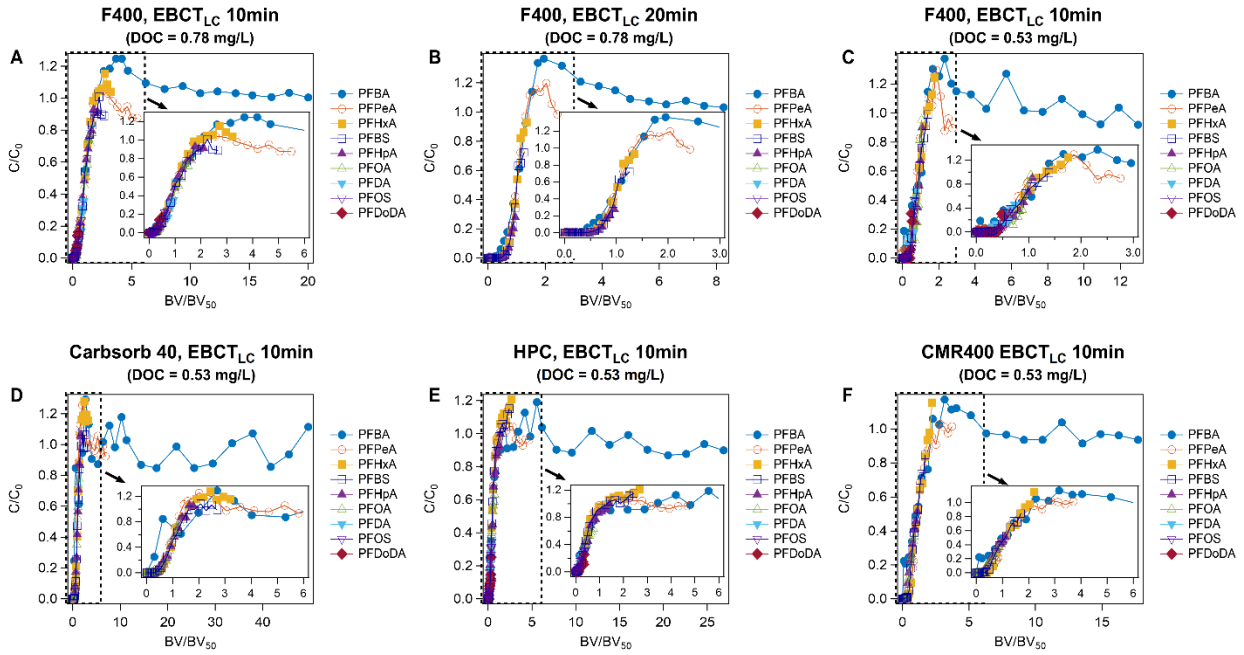

Fig. S8. Breakthrough curves of PFAS with respect to BV normalized by BV_{50}. DOC concentrations of the feed water were 0.78 mg/L and 0.53 m/L for the sampling campaign 1 (A and B) and 2 (C to F), respectively.

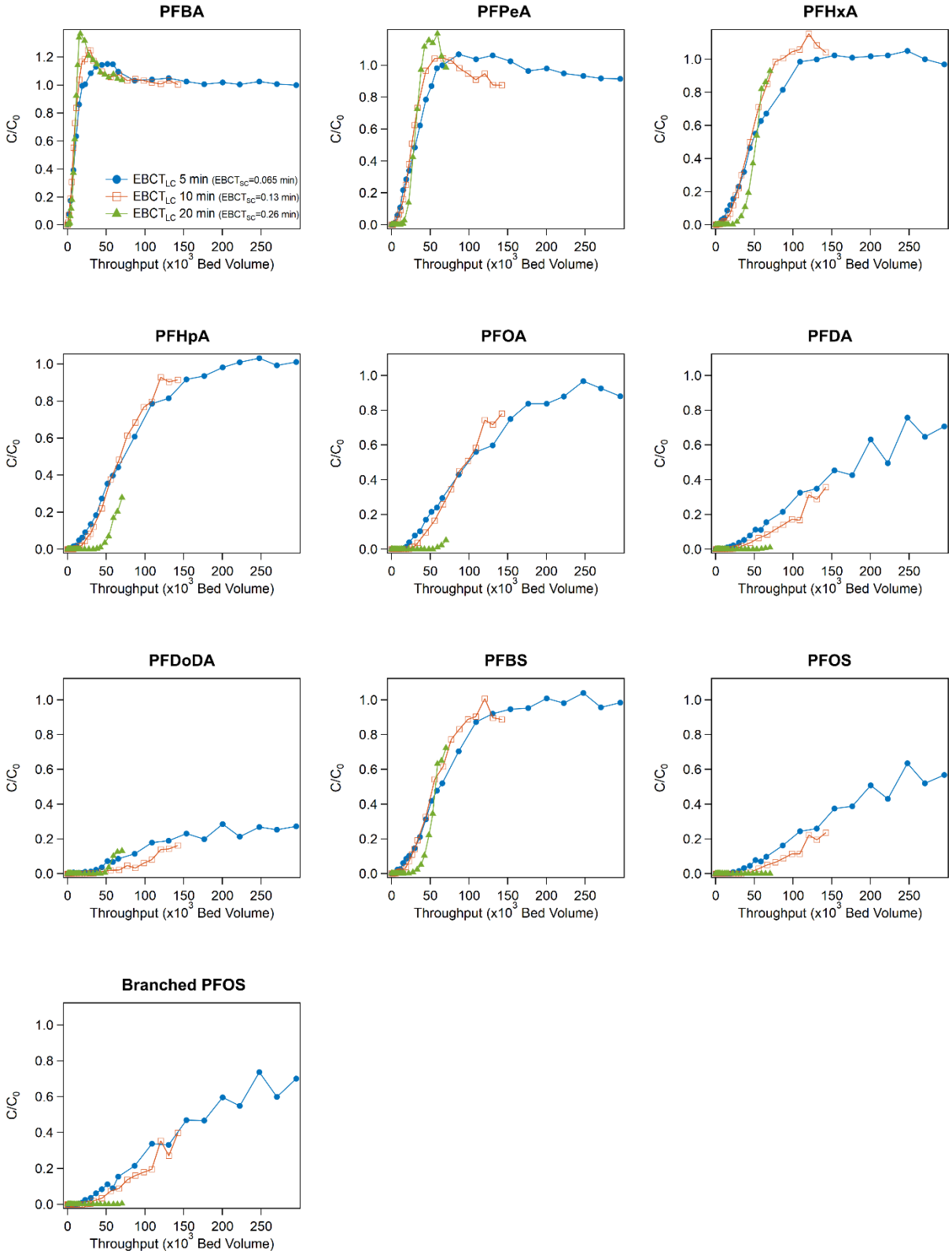
PFBA
PFPeA
PFHxA
PFHpA
PFOA
PFDA
PFDoDA
PFBS
PFOS
Branched PFOS
C/C0
Throughput (x10^3 Bed Volume)
EBCTLC 5 min (EBCTSC=0.065 min)
EBCTLC 10 min (EBCTSC=0.13 min)
EBCTLC 20 min (EBCTSC=0.26 min)

86

Fig. S9. Breakthrough curves of all the tested PFAS with respect to throughput for three different $EBCT_{LC}$ values (5 min, 10 min, and 20 min).

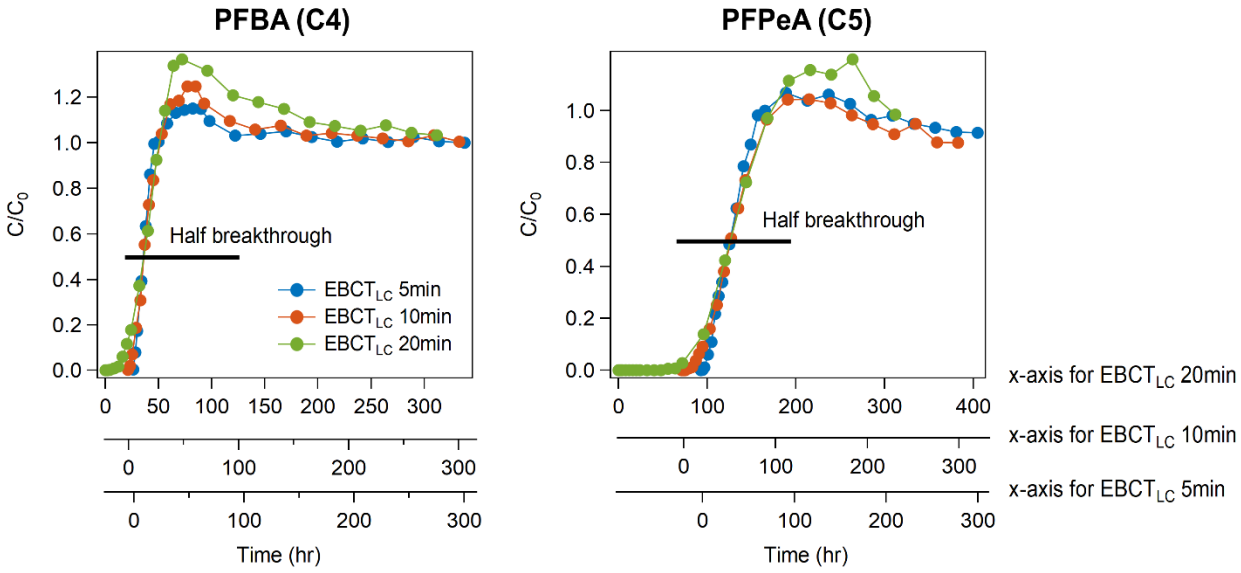

Fig. S10. The breakthrough curves of two hydrophilic PFAS. The breakthrough curves were shifted to Each breakthrough curve was shifted to match BV_{50} each other.

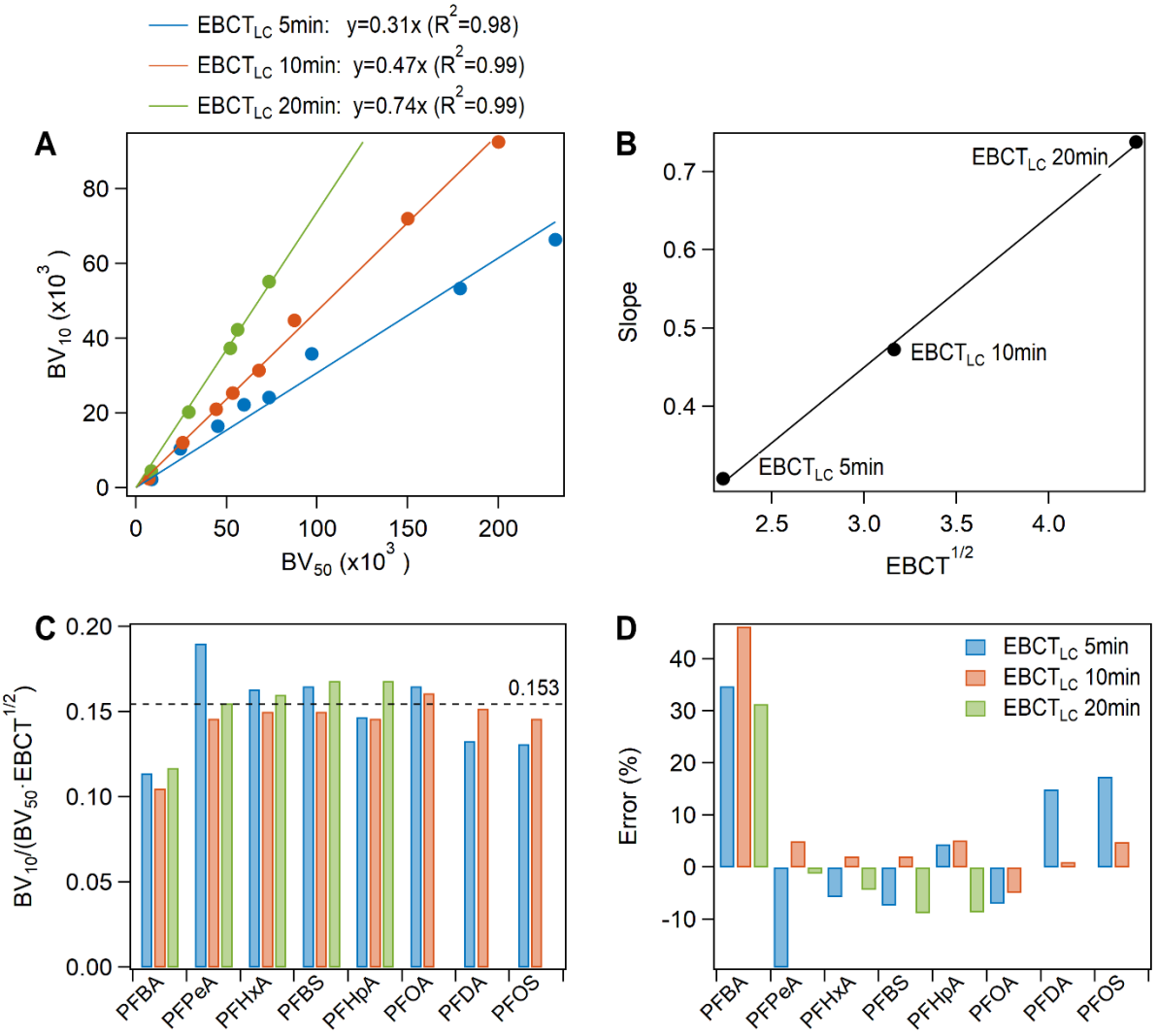

93

94 **Fig. S11**. The relation between BV_{10} and BV_{50} (A); the slope of BV_{10} versus BV_{50} with respect
95 to $EBCT^{1/2}$ (B); $BV_{10}/(BV_{50}\cdot EBCT^{1/2})$ (C); and percent error values of the estimated BV_{10} values
96 that were calculated by Eq. (1) (D). PFDoDA for all the $EBCT_{LC}$ values and PFOA, PFDA and
97 PFOS for 20 min of $EBCT_{LC}$ could not be estimated due to the lack of data points caused by very
98 shallow breakthrough trends.

99

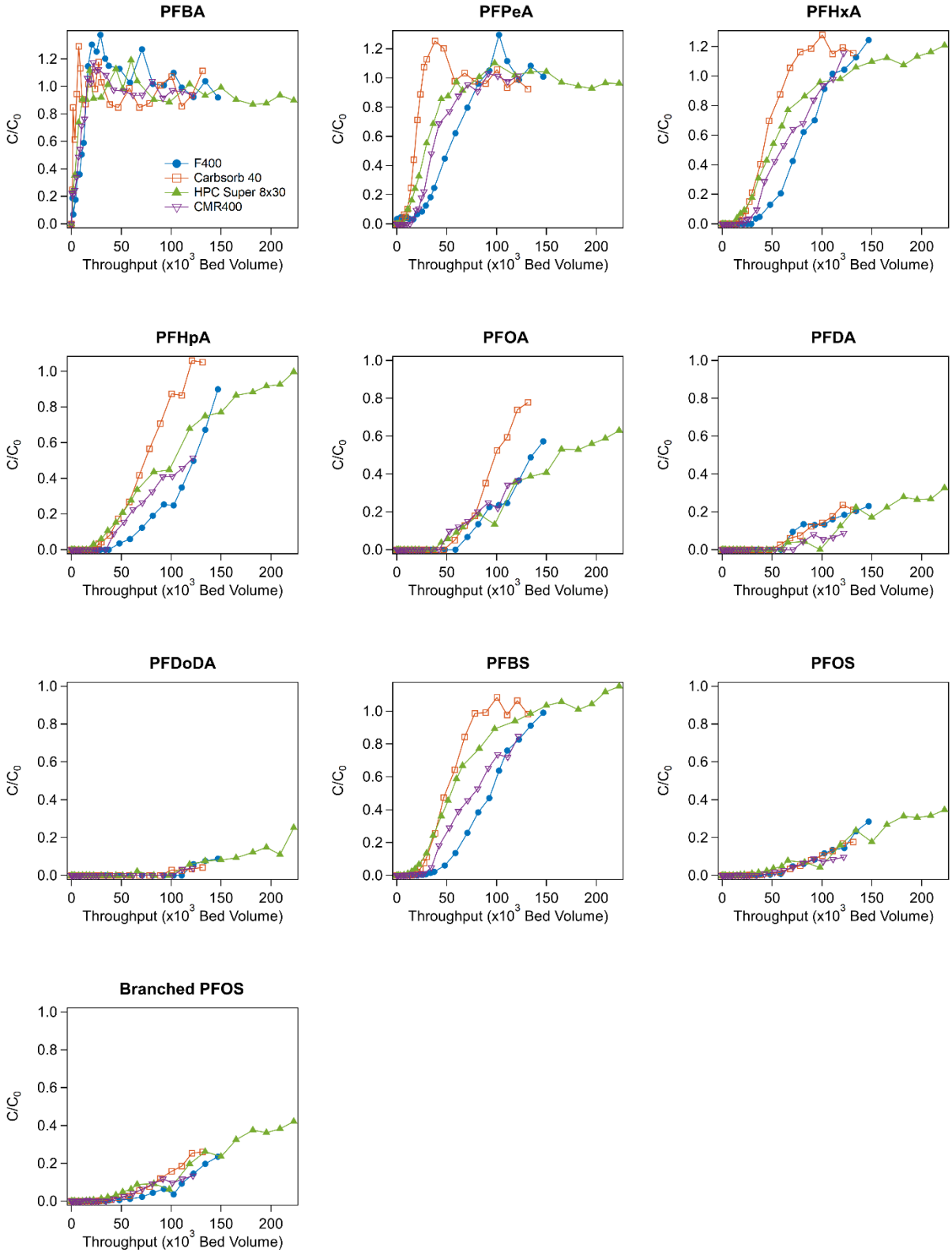
PFBA
PFPeA
PFHxA
PFHpA
PFOA
PFDA
PFDoDA
PFBS
PFOS
Branched PFOS
C/C0
Throughput (x10^3 Bed Volume)
F400
Carbsorb 40
HPC Super 8x30
CMR400

100

Fig. S12. Breakthrough curves of all the tested PFAS with respect to BV for four different activated carbons.

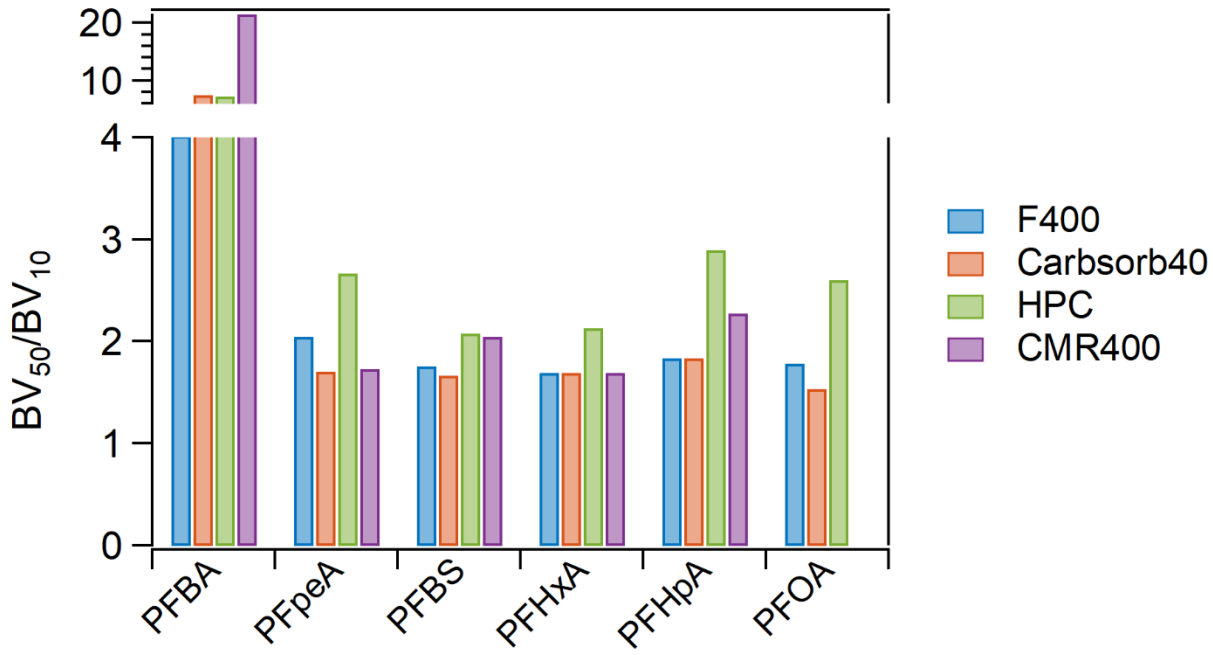

Fig. S13. Retention coefficients ($RC=BV_{50}/BV_{10}$) of the six selected PFAS. The RC of PFOA could not be achieved for CMR400 since half breakthrough was not achieved.

S6. References

Anumol, T., Sgroi, M., Park, M., Roccaro, P. and Snyder, S.A. (2015) Predicting trace organic compound breakthrough in granular activated carbon using fluorescence and UV absorbance as surrogates. Water Research 76(0), 76-87.

Appleman, T.D., Higgins, C.P., Quiñones, O., Vanderford, B.J., Kolstad, C., Zeigler-Holady, J.C. and Dickenson, E.R.V. (2014) Treatment of poly- and perfluoroalkyl substances in U.S. full-scale water treatment systems. Water Research 51, 246-255.

Athanasaki, G., Sherrill, L. and Hristovski, K.D. (2015) The pore surface diffusion model as a tool for rapid screening of novel nanomaterial-enhanced hybrid ion-exchange media. Environmental Science: Water Research & Technology 1(4), 448-456.

Carter, K.E. and Farrell, J. (2010) Removal of Perfluorooctane and Perfluorobutane Sulfonate from Water via Carbon Adsorption and Ion Exchange. Separation Science and Technology 45(6), 762-767.

Chowdhury, Z.K. (2013) Activated carbon: solutions for improving water quality, American Water Works Association.

Corwin, C.J. and Summers, R.S. (2010) Scaling Trace Organic Contaminant Adsorption Capacity by Granular Activated Carbon. Environmental Science & Technology 44(14), 5403-5408.

Corwin, C.J. and Summers, R.S. (2011) Adsorption and desorption of trace organic contaminants from granular activated carbon adsorbers after intermittent loading and throughout backwash cycles. Water Research 45(2), 417-426.

Cousins, I.T., Vestergren, R., Wang, Z., Scheringer, M. and McLachlan, M.S. (2016) The precautionary principle and chemicals management: The example of perfluoroalkyl acids in groundwater. Environment International 94, 331-340.

Crittenden, J., Berrigan, J., Hand, D. and Lykins, B. (1987) Design of Rapid Fixed-Bed Adsorption Tests for Nonconstant Diffusivities. Journal of Environmental Engineering 113(2), 243-259.

Crittenden, J.C., Berrigan, J.K. and Hand, D.W. (1986) Design of Rapid Small-Scale Adsorption Tests for a Constant Diffusivity. Journal (Water Pollution Control Federation) 58(4), 312-319.

Crittenden, J.C., Reddy, P.S., Arora, H., Trynoski, J., Hand, D.W., Perram, D.L. and Summers, R.S. (1991) Predicting GAC Performance With Rapid Small-Scale Column Tests. Journal (American Water Works Association) 83(1), 77-87.

Dastgheib, S.A., Karanfil, T. and Cheng, W. (2004) Tailoring activated carbons for enhanced removal of natural organic matter from natural waters. Carbon 42(3), 547-557.

EPA (2019) EPA's Per- and Polyfluoroalkyl Substances (PFAS) Action Plan.

Erkoç, Ş. and Erkoç, F. (2001) Structural and electronic properties of PFOS and LiPFOS. Journal of Molecular Structure: THEOCHEM 549(3), 289-293.

Eschauzier, C., Beerendonk, E., Scholte-Veenendaal, P. and De Voogt, P. (2012) Impact of Treatment Processes on the Removal of Perfluoroalkyl Acids from the Drinking Water Production Chain. Environmental Science & Technology 46(3), 1708-1715.

Hand, D., Crittenden, J., Hokanson, D. and Bulloch, J. (1997) Predicting the performance of fixed-bed granular activated carbon adsorbers. Water Science and Technology 35(7), 235-241.

Hansen, M.C., Børresen, M.H., Schlabach, M. and Cornelissen, G. (2010) Sorption of perfluorinated compounds from contaminated water to activated carbon. Journal of Soils and Sediments 10(2), 179-185.

Hashimoto, I., Deshpande, K. and Thomas, H.C. (1964) Peclet numbers and retardation factors for ion exchange columns. Industrial & Engineering Chemistry Fundamentals 3(3), 213-218.

Hu, X.C., Andrews, D.Q., Lindstrom, A.B., Bruton, T.A., Schaider, L.A., Grandjean, P., Lohmann, R., Carignan, C.C., Blum, A., Balan, S.A., Higgins, C.P. and Sunderland, E.M. (2016) Detection of Poly- and Perfluoroalkyl Substances (PFASs) in U.S. Drinking Water Linked to Industrial Sites, Military Fire Training Areas, and Wastewater Treatment Plants. Environmental Science & Technology Letters 3(10), 344-350.

Hutzler, N.J., Crittenden, J.C., Gierke, J.S. and Johnson, A.S. (1986) Transport of Organic Compounds With Saturated Groundwater Flow: Experimental Results. Water Resources Research 22(3), 285-295.

Karanfil, T. and Kilduff, J.E. (1999) Role of Granular Activated Carbon Surface Chemistry on the Adsorption of Organic Compounds. 1. Priority Pollutants. Environmental Science & Technology 33(18), 3217-3224.

Kennedy, A.M. and Summers, R.S. (2015) Effect of DOM Size on Organic Micropollutant Adsorption by GAC. Environmental Science & Technology 49(11), 6617-6624.

Li, Q., Snoeyink, V.L., Mariãas, B.J. and Campos, C. (2003) Elucidating competitive adsorption mechanisms of atrazine and NOM using model compounds. Water Research 37(4), 773-784.

Liu, C.J., Werner, D. and Bellona, C. (2019) Removal of per- and polyfluoroalkyl substances (PFASs) from contaminated groundwater using granular activated carbon: a pilot-scale study with breakthrough modeling. Environmental Science: Water Research & Technology.

McCleaf, P., Englund, S., Östlund, A., Lindegren, K., Wiberg, K. and Ahrens, L. (2017) Removal efficiency of multiple poly- and perfluoroalkyl substances (PFASs) in drinking water using granular activated carbon (GAC) and anion exchange (AE) column tests. Water Research 120, 77-87.

McNamara, J.D., Franco, R., Mimna, R. and Zappa, L. (2018) Comparison of Activated Carbons for Removal of Perfluorinated Compounds From Drinking Water. Journal - American Water Works Association 110(1), E2-E14.

Newcombe, G., Morrison, J., Hepplewhite, C. and Knappe, D.R.U. (2002) Simultaneous adsorption of MIB and NOM onto activated carbon: II. Competitive effects. Carbon 40(12), 2147-2156.

NJDEP (2018) Specific Ground Water Quality Criteria for 1,2,3-Trichloropropane (TCP) and Perfluorononanoic Acid (PFNA).

Pan, L., Takagi, Y., Matsui, Y., Matsushita, T. and Shirasaki, N. (2017) Micro-milling of spent granular activated carbon for its possible reuse as an adsorbent: Remaining capacity and characteristics. Water Research 114, 50-58.

Patterson, C., Burkhardt, J., Schupp, D., Krishnan, E.R., Dyment, S., Merritt, S., Zintek, L. and Kleinmaier, D. (2019) Effectiveness of point-of-use/point-of-entry systems to remove per- and polyfluoroalkyl substances from drinking water. AWWA Water Science 1(2).

Quiñones, O. and Snyder, S.A. (2009) Occurrence of Perfluoroalkyl Carboxylates and Sulfonates in Drinking Water Utilities and Related Waters from the United States. Environmental Science & Technology 43(24), 9089-9095.

Redding, A.M. and Cannon, F.S. (2014) The role of mesopores in MTBE removal with granular activated carbon. Water Research 56, 214-224.

Scheurer, M., Storck, F.R., Brauch, H.-J. and Lange, F.T. (2010) Performance of conventional multi-barrier drinking water treatment plants for the removal of four artificial sweeteners. Water Research 44(12), 3573-3584.

Senevirathna, S.T.M.L.D., Tanaka, S., Fujii, S., Kunacheva, C., Harada, H., Shivakoti, B.R. and Okamoto, R. (2010) A comparative study of adsorption of perfluorooctane sulfonate (PFOS) onto granular activated carbon, ion-exchange polymers and non-ion-exchange polymers. Chemosphere 80(6), 647-651.

Shih, T., Wangpaichitr, M. and Suffet, M. (2005) Performance and Cost Evaluations of Synthetic Resin Technology for the Removal of Methyl Tert-Butyl Ether from Drinking Water. Journal of Environmental Engineering 131(3), 450-460.

Shih, T.C., Wangpaichitr, M. and Suffet, M. (2003) Evaluation of granular activated carbon technology for the removal of methyl tertiary butyl ether (MTBE) from drinking water. Water Research 37(2), 375-385.

Siriwardena, D.P., Crimi, M., Holsen, T.M., Bellona, C., Divine, C. and Dickenson, E. (2019) Influence of groundwater conditions and co-contaminants on sorption of perfluoroalkyl compounds on granular activated carbon. Remediation Journal 29(3), 5-15.

Smith, R. and Tanford, C. (1973) Hydrophobicity of long chain n-alkyl carboxylic acids, as measured by their distribution between heptane and aqueous solutions. Proceedings of the National Academy of Sciences 70(2), 289-293.

Sontheimer, H., Crittenden, J.C. and Summers, R.S. (1988) Activated carbon for water treatment.

Sperlich, A., Werner, A., Genz, A., Amy, G., Worch, E. and Jekel, M. (2005) Breakthrough behavior of granular ferric hydroxide (GFH) fixed-bed adsorption filters: modeling and experimental approaches. Water Research 39(6), 1190-1198.

Summers, R.S., Kim, S.M., Shimabuku, K., Chae, S.-H. and Corwin, C.J. (2013) Granular activated carbon adsorption of MIB in the presence of dissolved organic matter. Water Research 47(10), 3507-3513.

Sun, M., Arevalo, E., Strynar, M., Lindstrom, A., Richardson, M., Kearns, B., Pickett, A., Smith, C. and Knappe, D.R.U. (2016) Legacy and Emerging Perfluoroalkyl Substances Are Important Drinking Water Contaminants in the Cape Fear River Watershed of North Carolina. Environmental Science & Technology Letters 3(12), 415-419.

SWRCB (2019) Perfluorooctanoic acid (PFOA) and Perfluorooctanesulfonic acid (PFOS).

Vanderford, B.J., Pearson, R.A., Rexing, D.J. and Snyder, S.A. (2003) Analysis of Endocrine Disruptors, Pharmaceuticals, and Personal Care Products in Water Using Liquid Chromatography/Tandem Mass Spectrometry. Analytical chemistry 75(22), 6265-6274.

Westerhoff, P., Highfield, D., Badruzzaman, M. and Yoon, Y. (2005) Rapid Small-Scale Column Tests for Arsenate Removal in Iron Oxide Packed Bed Columns. Journal of Environmental Engineering 131(2), 262-271.

Worch, E. (2008) Fixed-bed adsorption in drinking water treatment: a critical review on models and parameter estimation. Journal of Water Supply: Research and Technology-AQUA 57(3), 171-183.

Xiao, F., Zhang, X., Penn, L., Gulliver, J.S. and Simcik, M.F. (2011) Effects of Monovalent Cations on the Competitive Adsorption of Perfluoroalkyl Acids by Kaolinite: Experimental Studies and Modeling. Environmental Science & Technology 45(23), 10028-10035.

Xiao, X., Ulrich, B.A., Chen, B. and Higgins, C.P. (2017) Sorption of Poly- and Perfluoroalkyl Substances (PFASs) Relevant to Aqueous Film-Forming Foam (AFFF)-Impacted Groundwater by Biochars and Activated Carbon. Environmental Science & Technology 51(11), 6342-6351.

Yu, J., Lv, L., Lan, P., Zhang, S., Pan, B. and Zhang, W. (2012) Effect of effluent organic matter on the adsorption of perfluorinated compounds onto activated carbon. Journal of Hazardous Materials 225–226, 99-106.

Yu, Q., Zhang, R., Deng, S., Huang, J. and Yu, G. (2009) Sorption of perfluorooctane sulfonate and perfluorooctanoate on activated carbons and resin: Kinetic and isotherm study. Water Research 43(4), 1150-1158.